The effect of storms on the Antarctic Slope Current and the warm inflow onto the southeastern Weddell Sea continental shelf

Vår Dundas^{1,2}, Kjersti Daae¹, Elin Darelius¹, Markus Janout³, Jean-Baptiste Sallée⁴, and Svein Østerhus⁵

Correspondence: Vår Dundas (var.dundas@nersc.no)

Abstract. The southern Weddell Sea and Storms have been suggested to drive enhanced southward transport of modified Warm Deep Water (mWDW) towards the Filchner Ice Shelf eavity are locations Front in the southern Weddell Sea. This region is a known location of dense bottom water production and are thus connected is thus tightly linked to the global climate system. However, it has been suggested that increased heat transport from the deep ocean onto the continental shelf and towards the ice cavities would disrupt the could lead to higher ice shelf melt rates and disrupt dense water productionand increase ice shelf melt rates. Processes that affect. The role of storms and wind forcing in enhancing the southward heat transport are, therefore , important to understand. Sudden strong westward ocean surface stress events - "storms" - are suggested to drive enhanced southward transport of modified Warm Deep Water across the continental shelf-is therefore of interest. We utilize observational records spanning up to four years of data from a network of moorings deployed in the Filchner Trough region in the southeastern Weddell Sea. We use a mooring network with up to four-year-long mooring records from the region to to investigate how the regional ocean circulation responds to storm events. We find that about 70% of the events that last longer than four days, have a eumulative westward stress increase larger than, and a storm events that i) last sufficiently long (longer than 5.7 days), ii) have a large enough accumulation of ocean surface stress anomaly throughout the storm (larger than $0.9 \,\mathrm{N\,m^{-2}\,dav^{-1}}$), and iii) are severe enough at their peak intensity (maximum stress above leads 0.5 N m⁻²) lead to a significant increase in the speed of the Antarctic Slope Current (ASC) just upstream of Filchner Trough . Roughly one-third while roughly 25% of the identified storm events cause an events also cause increased southward current speed on the shelf at depths where mWDW is expected to be present during the summer and autumn. At the southernmost mooring (76°S, storm) storm-driven responses are observed mainly during the latter part of the record (mid-2019 to early 2021). This interannual variability in storm response indicates a potential dependency on background hydrography and circulation that remains to be fully explained. This study highlights the potential importance of storms for southward heat transporttowards the Antarctic ice shelves. Warm water that is present on the continental shelf during a storm will likely be pushed southward by the enhanced circulation, increasing the southward heat

¹Geophysical Institute, University of Bergen and the Bjerknes Centre for Climate Research, Alleg. 70, Bergen, Norway

²Nansen Environmental and Remote Sensing Center

³Alfred-Wegener-Institute Helmholtz Centre for Polar and Marine Research, Am Handelshafen 12, D-27570 Bremerhaven, Germany

⁴Sorbonne Université/CNRS/IRD/MNHN, LOCEAN-IPSL, Laboratoire d'Océanographie et du Climat: Expérimentation et Approches Numériques, Paris, France

⁵NORCE Norwegian Research Centre and Bjerknes Centre for Climate Research, Nygårdsgt 112, Bergen, Norway

transport and the likelihood that it reaches: an accelerated circulation on the shelf increases the likelihood for warm summer inflow to reach the ice shelf front and cavity before the heat is lost to the atmosphere during winter through winter convection.

1 Introduction

Strong ocean surface stress events - "storms" hereafter referred to as storms - are suggested have been suggested (Darelius et al., 2016; Dundas et al., 2024) to cause enhanced southward transport of modified Warm Deep Water (mWDW, \sim -1.5°C to 0.0°C, Nicholls et al., 2009) across the continental shelf in the southeastern Weddell Sea (Darelius et al., 2016; Dundas et al., 202 which is today. This shelf is currently characterized as a cold, dense shelf region (Thompson et al., 2018) with an outflow of dense Ice Shelf Water through Filchner Trough (Foldvik et al., 2004), Southward intrusions of mWDW, originating from the open ocean north of the continental shelf break (Ryan et al., 2016) (Arthun et al., 2012), are mostly limited to the summer sea-30 son when the thermocline at the shelf break is shallow (e.g., Darelius et al., 2024b; Årthun et al., 2012). These intrusion deep intrusions of mWDW onto the continental shelf extends up to roughly typically fill the water column below 300 m depth, creating a thick layer of warm waters below the cold surface waters (e.g., Steiger et al., 2024; Arthun et al., 2012). The warm water then propagates southward throughout fall, reaching 76S, autumn and reaches roughly halfway south to the Filchner Ice Shelf, Front several months later (Steiger et al., 2024; Ryan et al., 2017) (Steiger et al., 2024; Ryan et al., 2017; Sallée et al., 2024). 35 Darelius et al. (2016) suggested storms as a driver of that storms can drive particularly far-reaching intrusions of warm water. as they observed coincident events of strong, short-lived anomalies in wind speed and enhanced ocean currents carrying mWDW southward along the eastern flank of the Filchner Troughtoward the Filchner Ice front. In model studies, mWDW entering Filchner Trough. It has further been suggested that if mWDW consistently enters the Filchner Ice Shelf cavity along this path has been suggested to potentially cause the system to change into a warmer the system could shift from a cold to a warm regime with dramatically increased basal melt rates in the future (Hellmer et al., 2012, 2017). Enhanced basal melt affects sea level, deep water production and the hydrography on the continental shelf, deep water production, and, by extension, the global climate as well as sea level through reduced buttressing of continental ice flow into the ocean, and thus is of global importance (Orsi et al., 1999; Marshall and Speer, 2012; Jacobs, 2004). Given these implications, this study aims to deepen our understanding of how sudden strong wind events storms affect the circulation and the transport of heat in the southward heat transport in the Filchner Trough region.

A The strong horizontal density gradient known as characterizing the Antarctic Slope Front (ASF), separates the cold shelf waters from the warm water of the open ocean (e.g., Gill, 1973; Jacobs, 1991; Thompson et al., 2018). In the Weddell Sea, the ASF relaxes during summer due to weaker wind and stronger surface stratification (Hattermann, 2018; Daae et al., 2017) and allows warm water to access the continental shelf (e.g., Årthun et al., 2012; Ryan et al., 2017; Steiger et al., 2024). The persistent westward wind field (Hazel and Stewart, 2019) and the ASF support is associated with the strong westward Antarctic Slope Current (ASC, e.g., Thompson et al., 2018; Gill, 1973). The ASF and the ASC thus make up a strongly coupled system. The strong easterlies during winter Wintertime easterlies lead to Ekman convergence and coastal downwelling that will act to steepen the ASF and sustain a strong ASC (Thompson et al., 2018). The winds are generally weaker during summer

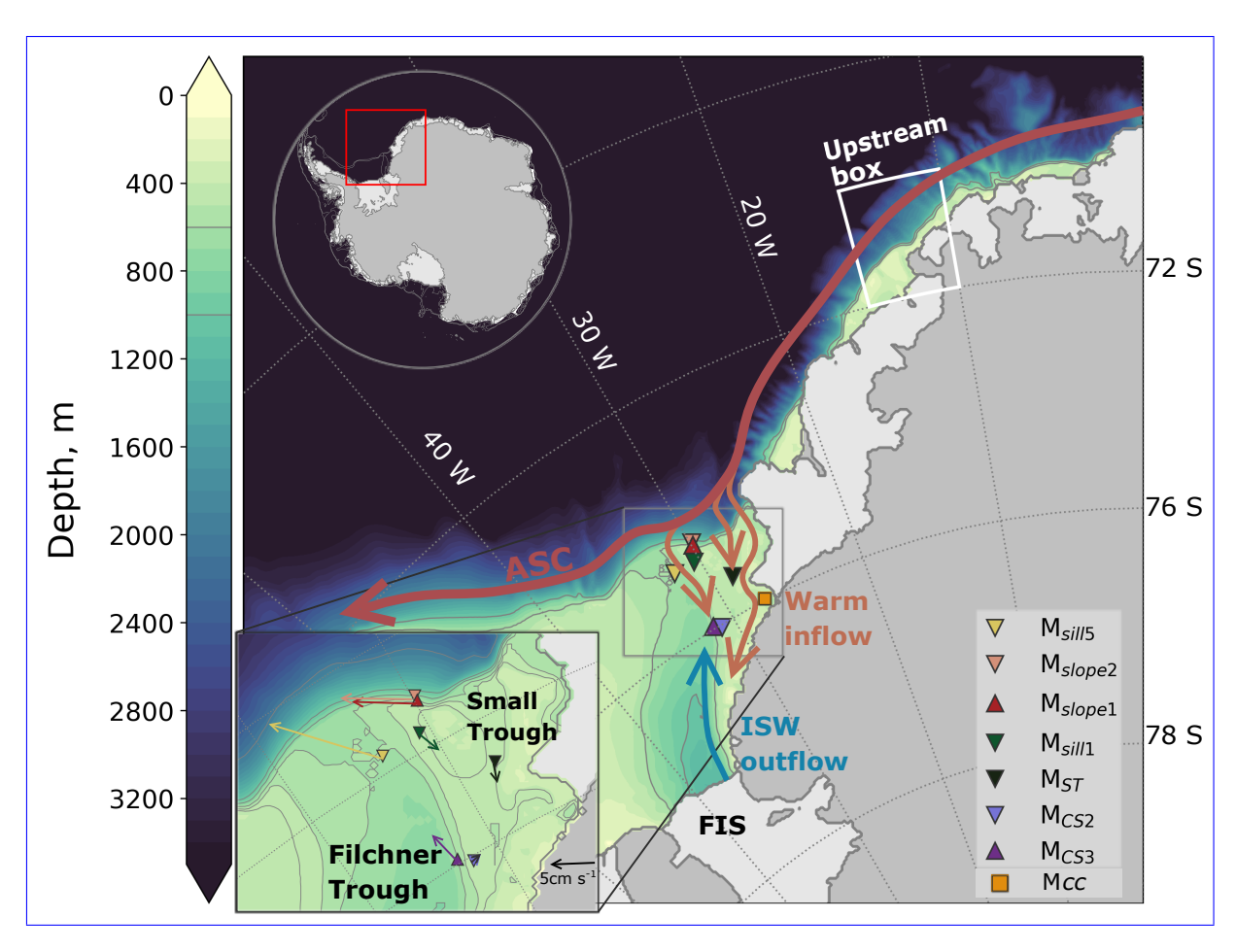


Figure 1. Bathymetry, Map over the ice shelves, and the ice sheet from Bedmap2 (Fretwell et al., 2013) with selected depth contours (gray lines on map and colorbar). The red box in the inset in the upper left corner indicates the study region. The area showing the mooring locations of , , , , , and are indicated by (colored markers. The orange square (M_{CC}) indicates, the location of a mooring that captured the Coastal Current from 2003 to 2004 (Daae et al., 2018; Nicholls, 2005). The inset in the lower left corner zooms in on the mooring locations main currents (Nicholls et al., 2009; Darelius et al., 2014) and shows their vertically averaged current, with a black scale arrow of 5 cm s⁻1. The white box (the "Upstream box") is used for estimates of to estimate the ocean surface stress. The bathymetry (color and gray contours) and the floating ice shelves (light gray) are from Bedmap2 (Fretwell et al., 2013). Filchner Trough, the Small Trough, and Filchner Ice Shelf (FIS)are labeled, and the main currents are indicated. The ASC Antarctic Slope Current (red arrowASC)and, the Coastal Current and warm inflow through Filchner Trough and the Ice Shelf Water (orange arrowsISW) outflow are based on Nicholls et al. (2009), while labeled. The red box in the northward ISW (blue arrow) is based on Darelius et al. (2014)upper inset indicates the study region. The lower inset shows the vertically averaged current at the mooring locations.

while the surface stratification is stronger (Hattermann, 2018). This allows for a relaxation of the ASF and a weaker ASC.

However, the In the Weddell Sea, the ASF relaxes during summer due to weaker wind and stronger surface stratification (Hattermann, 2018; Daae et al., 2017) and allows warm water to access the continental shelf (e.g., Årthun et al., 2012; Ryan et al., 2017; St

The relationship between the wind, the ASF, and the ASC is different on short time scales.

60

80

Sudden strong easterlies increase the Sea Surface Height subseasonal time scales: Strong easterlies associated with storm events increase the sea surface height (SSH) slope through Ekman transport towards the coast, which enhances the barotropic component of the ASC. This The storms, however, do not act sufficiently long to steepen the ASF. The increase in the barotropic component of the ASC is the main mechanism by which storms are suggested to enhance the heat transport towards the Filchner Ice Shelf cavity: a barotropically increased ASC due to storm-driven enhanced SSH-slope accelerates, as it strengthens the circulation on the shelf and moves accelerates the southward motion of warm waters already present on the continental shelf faster towards the south (Darelius et al., 2016; Dundas et al., 2024). The (Darelius et al., 2016; Dundas et al., 2024). In the current climate, the water column on the shelf is homogenized during winter (Ryan et al., 2017; Sallée et al., 2024), and all heat is lost to the atmosphere (Ryan et al., 2017), so the. The warm inflow must traverse the therefore traverse the roughly 400 km-wide continental shelf during the summer season if it is to reach the ice shelf front and the Filchner Ice Shelf cavity.

The deep Filchner Trough crosscuts the southeastern Weddell Sea continental shelf and acts as a southward gateway for mWDW towards the Filchner Ice Shelf cavity in the south (Fig. 1). At the mouth of Filchner Trough, the ASC bifurcates as the diverging isobaths steer a small branch of the current southward along the eastern flank of the trough (leftmost orange arrow in Fig. 1, e.g., Nicholls et al., 2009; Foldvik et al., 1985). Part of this southward-flowing current recirculates on the sill and joins the northward flow of Dense Shelf Water (DSW, Daae et al., 2017; Foldvik et al., 2004).

The remainder of the current continues south (e.g., Daae et al., 2017; Steiger et al., 2024), advecting warm mWDW southward along the eastern flank of Filchner Trough and onto the continental shelf east of the trough (e.g., Ryan et al., 2017; Darelius et al., 2016; Daae et al., 2020). Intrusions of mWDW have also been observed further east, as indicated by the two easternmost arrows in Fig. 1 (Steiger et al., 2024; Nicholls et al., 2009). In addition to the effect of the shelf break processes, this overall eirculation (Steiger et al., 2024; Nicholls et al., 2009; Sallée et al., 2024).

The circulation and hydrography in Filchner Trough is affected by large scale variability in the ice shelf cavity such as changes as the circulation below the Filchner-Ronne Ice Shelf shifts between the "Berkner" and "Ronne" modes of Ice Shelf Water production (ISW, below-freezing temperatures, e.g., Foldvik et al., 2004), where the The "Ronne"-mode is connected to enhanced ISW outflow characterized by large-scale cavity circulation and enhanced outflow of high-salinity Ronne-sourced ISW through Filchner Trough, while the "Berkner"-mode is characterized by more prominent local circulation and locally sourced ISW with lower source salinities (Hattermann et al., 2021; Janout et al., 2021).

Numerical experiments performed in an idealized setup of the Regional Ocean Modeling System (ROMS, Shchepetkin and McWilliams, Idealized numerical experiments support the hypothesis that storms ean enhance the southward heat transport as long as warm water is present by increasing the circulation on the continental shelf and the storm is sufficiently strong and long-lasting to eause a substantial increase in the circulation (Dundas et al., 2024). Previous mooring observations from the region, however,

90 (Dundas et al., 2024), but historical mooring records do not consistently show a relationship between southward transport and strong winds at 76S-wind (Ryan et al., 2017).

In this paper, we investigate how the circulation responds to strong wind forcing using up to four-year-long records of concurrent mooring data from the upper continental slope, the Filchner Trough sill, and the continental shelf east of the trough. We focus on this relationship and investigate the conditions during which strong ocean surface stress drives enhanced currents over storms drive enhanced currents along the slope and into Filchner Trough. We first using up to four-year-long records of concurrent mooring data. First, we present a case study that shows the current's potential response to a sudden, strong ocean surface stress event. Secondly, we look at composites of the response to the strong ocean surface stress events as well as the average and a composite analysis of the oceanic response to storms and the ambient atmospheric conditions during these events the storms. We then eonsider investigate why some events cause strongly enhanced currents while others do not and lastly, and finally, we briefly discuss a shift in hydrographic conditions and circulation that occurred during 2019, which appears to have impacted the potential of the ocean surface stress to cause strongly enhanced circulation on the southern part of the shelf. 2019. We, thus, provide new insights into the importance of storm events for the ASC and the southward heat transport in the Filchenr region and describe the nuances of why and when strong ocean surface stress events cause enhanced circulation in the regioncirculation on the continental shelf and attempt to determine when and why the events enhance the southward flow east of Filchner Trough.

2 Data and methods

100

105

110

120

2.1 Mooring records

We analyze velocity , temperature, and salinity records from seven-records from six moorings in the Filchner Trough region in the Southeastern Southeastern Weddell Sea (Fig. 1). The mooring names indicate their geographic location: M_{slope1} (Darelius et al., 2024a) and M_{slope2} (Darelius et al., 2023b) were positioned on the upper part of the continental slope, just north of the shelf beak, and captured the ASC just upstream of Filchner Trough. M_{sill5} (Østerhus, 2024) and M_{sill1} (Steiger et al., 2024) captured the outflow and inflow on across the Filchner Trough sill, respectively. M_{ST} (Steiger et al., 2024) was located in the trough just east of Filchner Trough, which we refer to as the "Small Trough" (Fig. 1). M_{CS2} (Darelius et al., 2023b) and M_{CS3} (Steiger et al., 2024) were located on the continental shelf on the eastern flank of Filchner Trough. The mooring locations are shown in Fig. 1, and their deployment details are given in Fig. 2 and Table 1. The mooring records span a varying period between 2017 and 2021, but their velocity records overlap for at least 20 months (Fig. 3).

We rotate the coordinate system at each mooring to align with the mean flow direction, which roughly aligns with the local isobaths (see Fig. 1), where a. A negative sign indicates current speed in the mean flow direction since the mean flows are roughly westward (M_{slope1} and M_{slope2}) and southward (M_{sill1} and M_{ST}). M_{CS2} and M_{sill5} are the exceptions: at. At M_{sill5} a positive sign indicates current in the main flow direction since the main flow direction is roughly northward, and at it is directed roughly northward. At M_{CS2} we align the coordinate system with the local isobaths (see Fig. 1) with as the mean

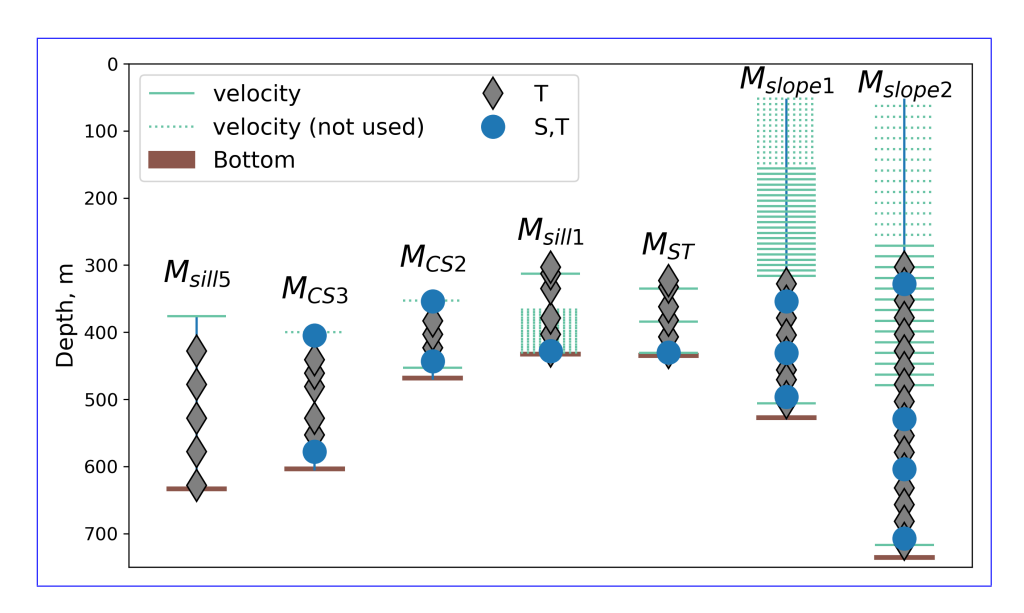


Figure 2. Sketch of the moorings indicating the depth of available observation depths with observational records according to the legend. Horizontal Tightly spaced turquoise lines indicate measurements of velocity. Frequent turquoise lines indicate ADCP measurements (Acoustic Doppler Current Profiler) bins $(M_{sill1}, M_{slope1}, and M_{slope2})$, and dotted lines indicate discarded bins. The brown horizontal line indicates the bottom.

current direction shifts (Ryan et al., 2017, and Fig. 1). After rotation, a negative sign indicates flow towards the southwest.

All analyses are carried out using hourly mean velocity records: we interpolate the data from. The moorings M_{slope2}, M_{CS2}, and M_{sill5}, which are on a two-hourly frequency, had a sampling interval of two hours for velocity; these records were linearly interpolated onto hourly time steps.

For moorings with high vertical resolution. Where possible, we have used the depth averaged current as we expect the storm response to be mainly barotropic (M_{slope1} , M_{slope2} , M_{ST}), we base the analysis on depth-averaged currents. At M_{sill1} where the time series from one level is significantly longer than the others we chose to include only data from that level. At mooring M_{CS2} , the currents at the upper instrument are weak and erratic, and we chose to include only the lower level. The levels included are marked in Fig. 2. At M_{slope1} and M_{slope2} , the data quality of the upper bins is poor during winter (due to too few scattering particles), and we've discarded levels with less than 43% data coverageat and. Data gaps shorter than six hours are filled by linear interpolation. The bottom sensor (Fig. 2) at both these moorings, which had the highest data quality and the strongest current (Darelius et al., 2024a), stopped recording in June 2019. For moorings with varying record lengths at different depths (), we use the data with the longest time series, and for the moorings with strong vertical variability (), we use the depth with the highest velocities.

130

135

While velocity is the main variable in this study, temperature and salinity are used in parts of the analysis. Data from a seventh mooring, M_{CS3} , located just west of M_{CS2} along the eastern slope of Filchner Trough is included when discussing

Table 1. Overview of the moorings. The indicated significance values limits (Section 2.5) for storm response are negative for all moorings except M_{sill5} because their main observed flow directions are have a strong westward or southward component. The significance value at M_{sill5} is positive because the main flow direction is has a strong northward component. No significance value is indicated for M_{CS3} because this mooring is dominated by northward flowing ISW and not used in the storm response analysis. Information about instruments, calibration, and data processing can be found in the indicated data reference.

heightMooring	Original	Deployment/	Lon/	Bottom	Significance	<u>Data</u>
name	name	Recovery	Lat	depth [m]	value [cm s^{-1}]	reference
M_{slope2} (UiB)	M3	24.02.2017	29°54.48'W	740	-9.06 - <u>8.72</u>	Darelius et al. (2023)
		14.02.2021	74°33.00'S			
M_{slope1} (UiB)	M6	24.02.2017	29°54.97'W	530	-7.64 - <u>7.88</u>	Darelius et al. (2024)
		13.02.2021	74°35.70'S			
$M_{\it sill}$ (LOCEAN)	P4	11.02.2017	30°23.01'W	435	-6.01 - <u>6.83</u>	Steiger and JB. (2023)
		15.02.2021	74°51.00'S			
M_{ST} (LOCEAN)	P5	09.02.2017	28°38.22'W	437	-5.67 - <u>6.92</u>	Steiger and JB. (2023)
		09.03.2021	75°23.38'S			
$M_{\it sill5}$ (NORCE)	S2	07.02.2018	31°49.84'W	636	17.75 - <u>18.31</u>	Østerhus (2024)
		16.02.2021	74°51.32'S			
${\rm M}_{CS2}$ (AWI)	A253-3	05.02.2018	31°01.42′W	471	-7.26 - <u>6.26</u>	Janout et al. (2022)
		01.03.2021	76°02.74'S			
${\rm M}_{CS3}$ (AWI)	A253-4-A254-3	05.02.2018	31°29.79'W	606	N/A	Janout et al. (2022)
		02.03.2021	75°57.68'S			

the shift from Ronne to Berkner mode (Fig. 2, Section C). We present temperature and salinity as conservative temperature, Θ, and absolute salinity, S_A, following TEOS-10, unless otherwise stated. We use the Gibbs seawater package for Python in conversions (McDougall and Barker, 2011).

2.2 Estimation of ocean surface stress

Ocean surface stress is estimated following Dotto et al. (2018), who estimate the air-ocean stress and ice-ocean stress separately and then combine them as fractions of the sea ice concentration as follows:

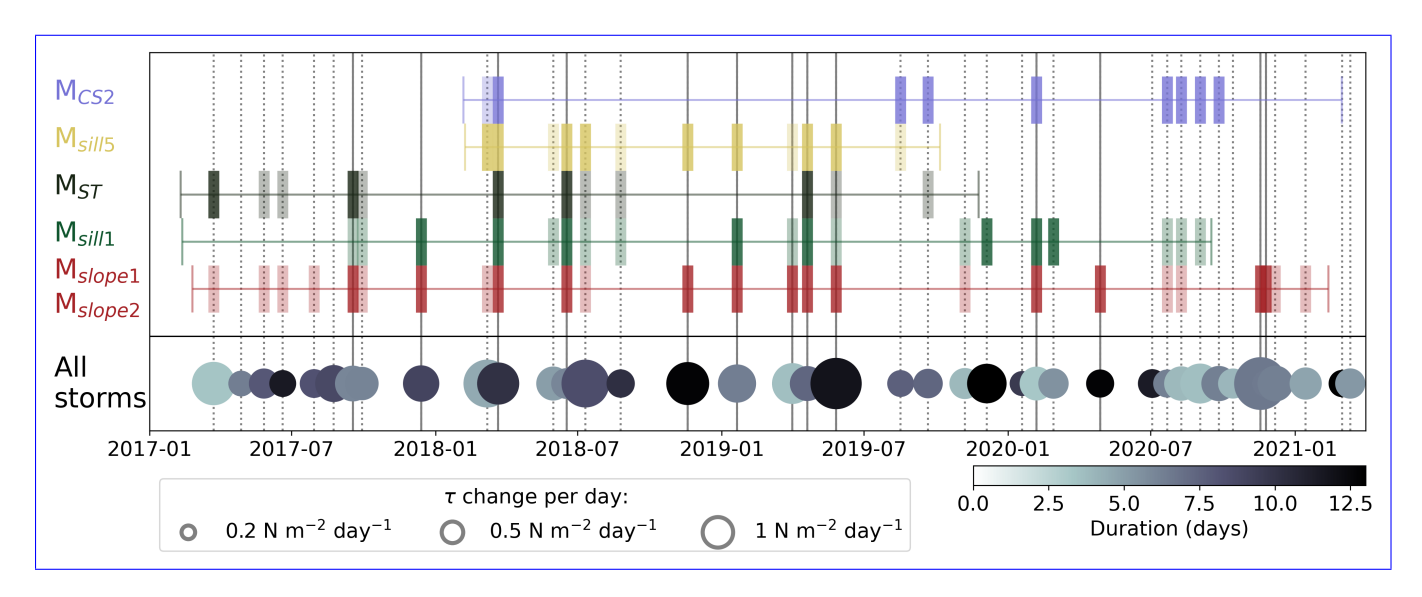


Figure 3. Overview of storms (dashed and solid vertical black lines) and storm responses (colored vertical bars) at the moorings. Horizontal lines show the duration of the mooring records, and dark colored vertical bars indicate a significant storm response. Light vertical bars show storm responses stronger than the 70^{th} percentile of background current increase (see methods 2.5). Storms with a significant response at both M_{slope1} and M_{slope2} are shown as solid, black vertical lines. The gray circles indicate the duration (color) and change in ocean surface stress, τ , per day (size) for the identified storms.

145
$$\overrightarrow{\tau} = \alpha \overrightarrow{\tau}_{ice-water} + (1 - \alpha) \overrightarrow{\tau}_{air-water},$$
 (1)

$$\overrightarrow{\mathcal{T}}_{ice-water} = \rho_{water} C_{iw} | \overrightarrow{U}_{ice} | \overrightarrow{U}_{ice}, \quad \text{and}$$
(2)

$$\overrightarrow{\tau}_{air-water} = \rho_{air} C_d |\overrightarrow{U}_{air}| \overrightarrow{U}_{air}.$$
(3)

(4)

Here α is the sea ice concentration, $\rho_{water} = 1028 \,\mathrm{kg} \,\mathrm{m}^{-3}$, $\rho_{air} = 1.25 \,\mathrm{kg} \,\mathrm{m}^{-3}$ are the densities of water and air, and $C_d = 1.25 \times 10^{-3}$ 150 and $C_{iw} = 5.50 \times 10^{-3}$ are the drag coefficients between air and ocean and ice and ocean, respectively. \overrightarrow{U}_{ice} and \overrightarrow{U}_{air} are the velocities of the ice and the air. The coordinate system is rotated 30° counterclockwise to roughly align with the coast in the Upstream box, and we use the along-slope component of the ocean surface stress in the following analysis.

2.3 Atmospheric and sea ice data

We use 10 m wind velocity, sea ice concentration(SIC), and mean sea level pressure from ERA5 (Hersbach et al., 2023). In estimations of the ocean surface stress, \(\tilde{\tau}\) (Eq. 4) used to identify storm events during the mooring period (Fig. 4), we use three-hourly 10 m wind and sea ice concentration from ERA5 over a region upstream of Filchner Trough ("Upstream box",

Fig. 1). For the maps in Figures 5-6 and 9, we use daily averaged output from ERA5. The anomalies of wind velocity and mean sea level pressure in Figure 6a,b) are referenced to monthly averaged March fields from 1990 to 2023. The sea ice concentration is referenced to the monthly climatology (average over the past 30 years), linearly interpolated onto daily values.

To estimate the ocean surface stress, $\overrightarrow{\tau}$, we average the three-hourly 10m wind and SIC over a region upstream of Filchner Trough ("Upstream box", Fig. 1). We chose this region because upstream wind forcing has been found to drive variability in circulation in this and similar regions on longer time scales (Daae et al., 2018; Lauber et al., 2023). Since we investigate the effect of sudden strong ocean surface stress events, we make the Upstream box relatively small – we want to avoid smoothing out maximum stress values. To estimate the sensitivity to the choice of box, we estimate the correlation between the wind speed averaged over the Upstream box and the wind speed in the surrounding regions (Fig. A2). The correlation is high in a large region surrounding the Upstream box, so we infer that the sensitivity to the exact choice of the box is small.

Ocean surface stress is estimated following Dotto et al. (2018), which estimates the air-ocean stress and ice-ocean stress separately and then combines these stresses as fractions of the SIC as follows:

170
$$\overrightarrow{\tau}_{ice-water} = \rho_{water} C_{iw} | \overrightarrow{U}_{ice}| \overrightarrow{U}_{ice}, \text{ and}$$

$$\overrightarrow{\tau}_{air-water} = \rho_{air} C_d | \overrightarrow{U}_{air}| \overrightarrow{U}_{air},$$

160

165

175

180

where α is the SIC, $\rho_{water} =$, $\rho_{air} =$, $C_d = 1.25 \times 10^{-3}$ We consider the ERA5 reanalysis a suitable data source for our purposes, as in situ observations are sparse and have limited spatial coverage. Caton Harrison et al. (2022) conducted a detailed comparison of coastal easterlies in three reanalysis products with satellite and in situ observations and concluded that ERA5 has the overall best performance. However, ERA5 underestimates coastal wind and $C_{iw} = 5.50 \times 10^{-3}$ are the drag coefficients between air and ocean and ice and ocean, respectively, and \overrightarrow{U}_{ice} and \overrightarrow{U}_{air} are the velocities of the ice and the airwind speeds exceeding $20\,\mathrm{m\,s^{-1}}$ in this region (Caton Harrison et al., 2022). It is therefore possible that the strongest wind events identified during our study period are underestimated in magnitude.

We use sea ice motion from the Upstream box (Fig. 1). The sea ice motion data is from NSIDC (Tschudi et al., 2019a) and stored is available on the 25km EASE-Grid (NSIDC, 2019). We , thus, average over the grid cells that overlap with the Upstream box and convert the data to northward apply a rotational matrix to obtain the north and eastward components by applying a rotational matrix as described in the data set's user resources (NSIDC, 2024) to estimate the NSIDC (2024).

2.4 Identification of "storm" events

185 The following procedure is used to identify events of strong ocean surface stress—

The records of westward, "storms". We de-trend the records of along-slope ocean surface stress are de-trended and then and apply a high-pass filtered using a fourth-filter (4th order 180 day Butterworth filterto remove) to remove the seasonality.

We then identify storm events as periods when the cumulative stress increases monotonically for more than 12h and where the total increase is at least . We combine two storm events into one $3.5\,\mathrm{N\,m^{-2}}$. We thus disregard the shortest and weakest wind events from further analysis, as we do not expect them to cause increased circulation (Dundas et al., 2024). Two storm events are combined if they are less than 15 hours apart. This condition is based on idealized model results from Dundas et al. (2024), which indicates that the circulation increases throughout the storm duration and stays enhanced for a few days after the storm has passed (Dundas et al., 2024). This means that a storm that occurs shortly after another adds momentum to an already enhanced current field. With this algorithm, we disregard the shortest and weakest wind events from further analysis, as we do not expect them to cause increased circulation (Dundas et al., 2024).

We use the cumulative ocean surface stress instead of the ocean surface stress directly because of the highly variable nature of the raw ocean surface stress signal. To avoid identifying a large number of events above a chosen ocean surface stress threshold a record. Alternatively, we could have used a low-pass filter would have to be applied, which makes but that would make the identification of storm start and end imprecise. The benefit of our procedure This is illustrated in Fig. A1a,b.

The "Upstream box" was chosen because upstream wind forcing has been found to drive variability in circulation in this and similar regions on longer timescales (Daae et al., 2018; Lauber et al., 2023). The wind-speed variability in the Upstream box is representative of the conditions in a large area surrounding the box (Fig. A2). A comparison of storm events identified using the Upstream box and a more local box (Fig. A3) gave similar but slightly poorer coherence between storm events and storm response at the slope moorings for the local box. The variability in the ASC strength observed at the slope moorings is relatively high and caused by e.g. baroclinic eddies, continental shelf waves Jensen et al. (2013), and remote wind forcing (Webb et al., 2019). We therefore do not expect to explain all ASC variability by using our Upstream box, but rather aim to identify regionally forced peaks in ASC strength.

2.5 Significant storm response

190

200

205

We need a definition of the current's define the "storm response" and an algorithm to evaluate whether an increase in ocean circulation is associated with a storm event or part of the background variability. The procedure is as the increase in current strength following a storm and quantify it as described below and illustrated in Fig. A1d. Prior to the analysis, the current records are low-pass filtered using a fourth 4th order Butterworth filter with a cut-off at 40h to remove shelf waves (Jensen et al., 2013) and tides.

We find that the largest current anomalies generally occur after the maximum ocean surface stress, τ_{max} . Therefore, for For each storm, we estimate the increase in current strength relative to the determine the time $(t=t_0)$ of maximum ocean surface stress, τ_{max} (sketch in Fig. A1d). We and we identify the maximum current strength during a ten-day period spanning three days before to prior to and seven days after τ_{max} ($U_{max}(t_0-3\text{days}:t_0+7\text{days})$). This maximum current is compared with the average current two days before the ten-day period ($U_{mean}(t_0-5\text{days}:t_0-3\text{days})$). We define the difference between the two-day average and the maximum current as the current's "storm response" ($U_{response}$, Fig. A1d),

220
$$U_{response} = U_{max}(t_0 - 3 \, \text{days} : t_0 + 7 \, \text{days}) - U_{mean}(t_0 - 5 \, \text{days} : t_0 - 3 \, \text{days})$$
 (5)

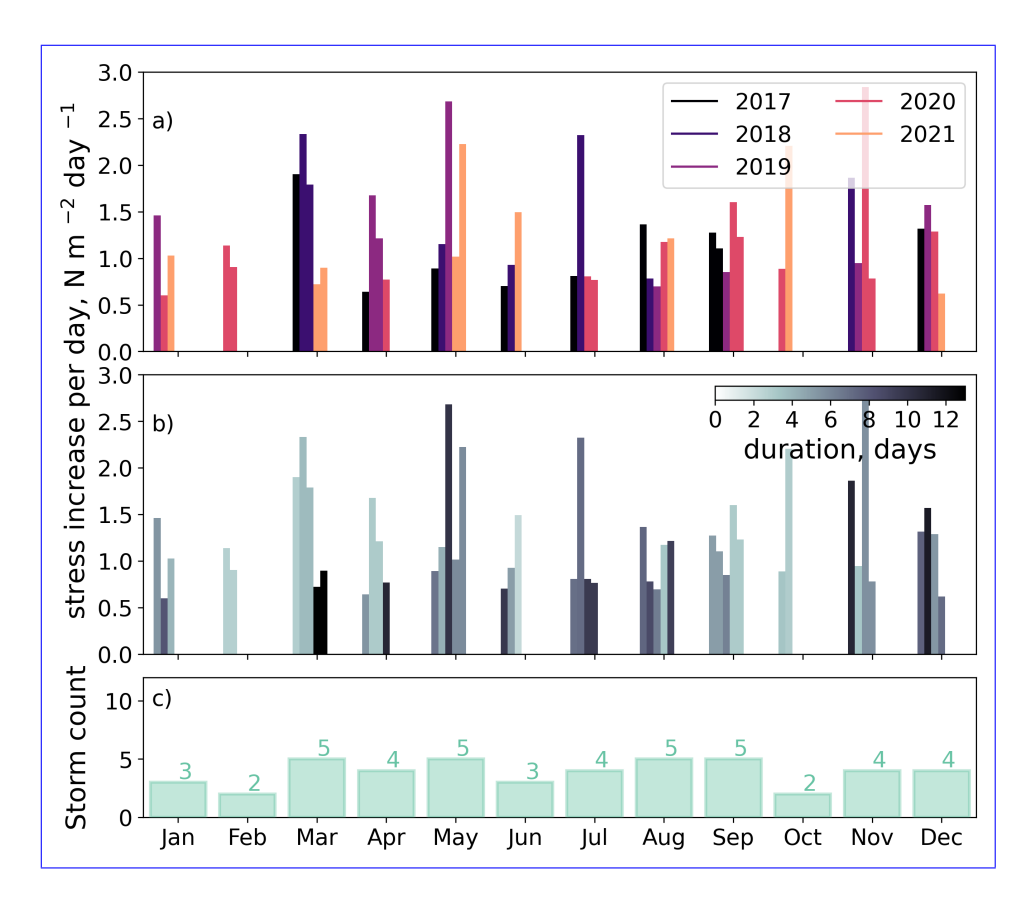


Figure 4. Distribution of storms throughout the mooring period (February Storm statistics between January 2017 to February 2021). and December 2021. Panels a) and b) show the increase in ocean surface stress per day for each the identified storm on the y-axis, with a) year and b) storm duration in color. c) shows the total storm count number of storms per month.

To assess whether a storm response is significant, we compare the responses with the current increase during 10-day longic, whether the observed increase in current strength exceeds the background variability, we use a Monte-Carlo-like approach. We cannot conduct a traditional Monte-Carlo procedure due to the length of the storm events relative to the length of the time series — the overlap between sample periods would be too large to act as randomized tests. Instead, we estimate the current increase $(U_{response})$ during all 10-day-long, 50% overlapping, storm-free windows . If a storm response (an example for M_{slope1} is shown in Fig. A1c). If $U_{response}$ during a storm is higher than the 90th percentile of these $U_{response}$ during the non-storm periods , we consider the storm response significant (example for (vertical blue line in Fig. A1c). Each mooring consequently , we consider the storm response significant. Each mooring has its own threshold for significance due to differences in the background variability (Table 2). The number of 10-day-long storm-free periods ranges from 88 to 213. 96 to 215.

2.6 Source salinity estimates

225

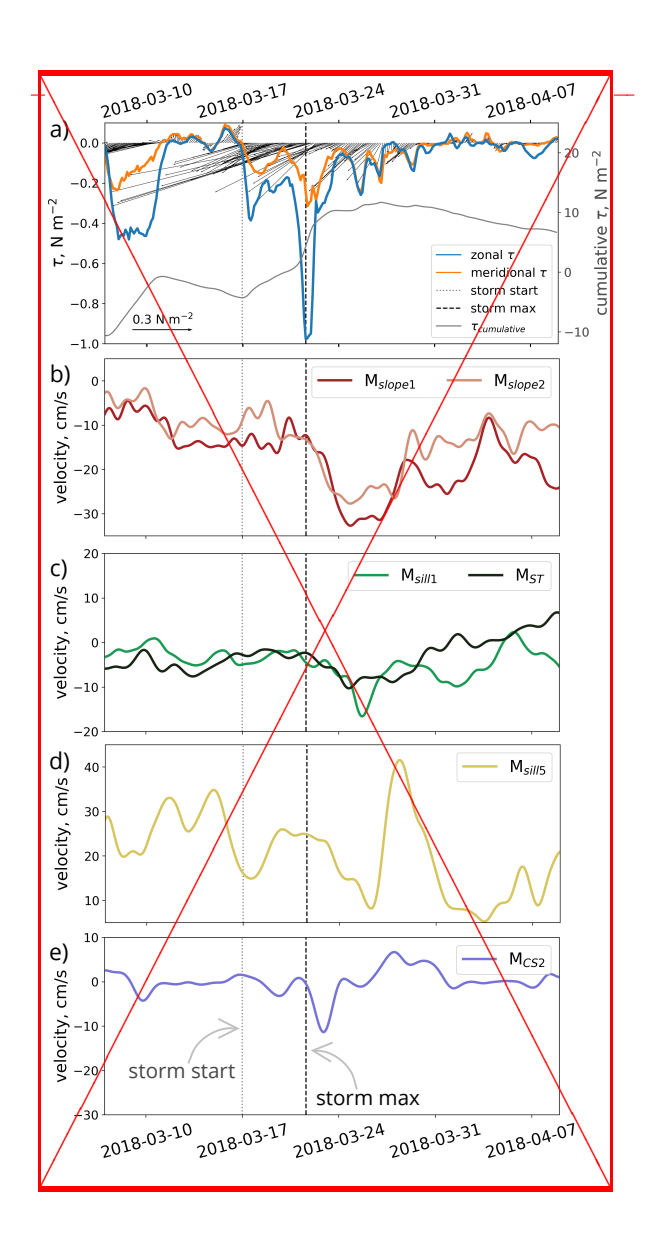
230

To estimate the arrival of the shift from Berkner to Ronne mode described by Hattermann et al. (2021) and Janout et al. (2021), we estimate the source salinity of the waters at by identifying the intersection between the Gade line (Gade, 1979) and the surface freezing point in ΘS_A space (illustrated in Fig. C1). Solving the linear relationship given by Wåhlin et al. (2010) for the source salinity, S_0 , gives

235
$$S_0 = S \left[1 + \frac{cp}{L_f} (T_0 - T) \right],$$

where $cp = 4186 \text{ J kg}^{-1} \text{ K}^{-1}$ and $L_f = 3.34 \times 10^5 \text{ J kg}^{-1}$. By first estimating the surface freezing temperature, T_0 , at the recorded salinity, S_0 , and then using Eq. C1 to estimate the corresponding source salinity, S_0 , we obtain an initial estimate of where the salinity-dependent surface freezing point intersects with the Gade line. The calculation is repeated once, replacing S_0 by S_0 to find a new T_0 and S_0 (Fig. C1).

The duration of mooring records (horizontal colored lines) with colored vertical bars indicating a significant storm response. The vertical black solid lines indicate a significant response at both and, while vertical dotted lines indicate storms that do not give a significant response at and. The grayscale circles at the bottom indicate the duration (color) and change in ocean surface stress, τ , per day (size) for the identified storms.



245 3 Results and discussion

250

We identify 41 strong wind 38 strong ocean surface stress events that we classify as "storms" between February 2017 and February 2021 (Fig. 3). The storms are spread-distributed relatively evenly throughout the four years, though the strongest and longest storms occur during fall spring and autumn (Fig. 4). All moorings consequently experience several storm events, and even the M_{sill5} mooring, which has the shortest record length (20 months), experiences 17–13 storms (Fig. 3). We find that while multiple many of the storms cause a significant response in the circulation at many of at the mooring locations, several other storms do not (Fig. 3). Additionally, several storms cause a significant response at some of the mooring locations but not at all of them (Fig. 3).

3.1 Case study: Storm-driven circulation increase at all moorings

255

260

265

275

280

We select a long (10 days) and present a case study of a particularly strong ($\tau_{max} = 1 \,\mathrm{N\,m^{-2}}$) storm and long-lasting (10 days) storm event in March 2018 to provide an example of how a storm can affect the current at the that affected all the mooring locations (Fig. 5a). We choose this storm because it is particularly strong and thus provides an example of how the circulation reacts to intense surface forcing.

The storm response at M_{slope2} and M_{slope1} is associated with an increase of the ASC of roughly $15\,\mathrm{cm\,s^{-1}}$, that lasts for four days and occurs directly after the maximum peak in ocean surface stress, and the current is enhanced by roughly westward (Fig. 5b)for about four days. At both M_{sill1} on the eastern flank of the sill and M_{ST} in the Small Trough, the response is significant, although it lasts shorter associated with a significant increased of the southward current a few days after the storm maximum, although the ocean current anomaly is shorter than at the slope (1-2 days, Fig. 5c). At M_{sill5} , the storm causes a significant northward response (i.e. an increased increase in the outflow of DSW (Fig. 5d), although this is the high variability during the storm period at this mooring makes this less evident in Fig. 5d relative to than at the other mooring locations due to the high variability during the storm period at .

. At M_{CS2} , along the eastern flank of Filchner Trough at 76°S, the southward storm response reaches $10 \,\mathrm{cm}\,\mathrm{s}^{-1}$, and the maximum current occurs shortly after the maximum stress during the storm ocean stress (Fig. 5e).

The atmospheric and sea ice conditions during the storm that started on the 17^{th} of March 2018 and reached maximum ocean surface stress, τ_{max} , on the 22^{th} of March. Anomalies of the a) mean sea level pressure with $10\,\mathrm{m}$ wind velocity vectors and b) absolute $10\,\mathrm{m}$ wind speed averaged ± 3 days of τ_{max} relative to the average March field (1990-2023). e) SIC averaged over the two days before the storm starts relative to the SIC climatology (past 30 years). d) Sea ice movement (Tschudi et al., 2019b) averaged ± 3 days of τ_{max} . White regions indicate missing data or no sea ice. In a,b), the Upstream box and the region shown in e,d) are indicated, and in e,d), the $1000\,\mathrm{m}$ and $600\,\mathrm{m}$ isobaths are indicated by gray lines (Fretwell et al., 2013). All SIC, pressure, and $10\,\mathrm{m}$ wind data are from ERA5 (Hersbach et al., 2023).

This storm, which gives a clear current response all the way south at M_{CS2} , is caused by a large low-pressure system positioned over the southern Weddell Sea (Fig. 5f6a). The cyclonic circulation of the low-pressure system hugs the coastline, creating a patch of anomalously high along-coast wind speeds stretching from roughly 30°W to 20°E (Fig. 5g6b). During the three days before and after τ_{max} , the high wind speed builds up and dies down without an evident along-coast propagation (not shown). The average SIC sea ice concentration on the eastern continental shelf and upstream of the trough is lower than the sea ice climatology, and the sea ice movement is relatively high over the continental shelf break (Fig. 5h,i). We hypothesize that the location and structure of the low-pressure system are important for the resulting oceanic response. It also emphasizes the effect of 6c.d). This case study emphasizes the remote effect that upstream ocean surface stress conditions can have on the local Filchner Trough circulation, in agreement with, e.g., Daae et al. (2018) and Lauber et al. (2023).

3.2 Composite analysis: the mean storm response

Pollowing the case study, which provides evidence Our case study suggests that a storm can cause both an enhanced ASC and enhanced eurrent currents far south along the flank of both Filchner Trough and the Small Trough, we. We, therefore, conduct a composite analysis of the eurrent at the moorings during all the identified storms. We group the composites into two classes: those mooring records using the identified storms to determine the mean storm response. For each mooring we make two composites: one for storms that give a significant response and those storm response at the mooring and one for storms that do not. The composites give several consistent indications of the effect of a storm event on the circulation at the moorings.

At and Our results are sensitive to the choice of threshold for a significant storm response (held at the 90th percentile of current

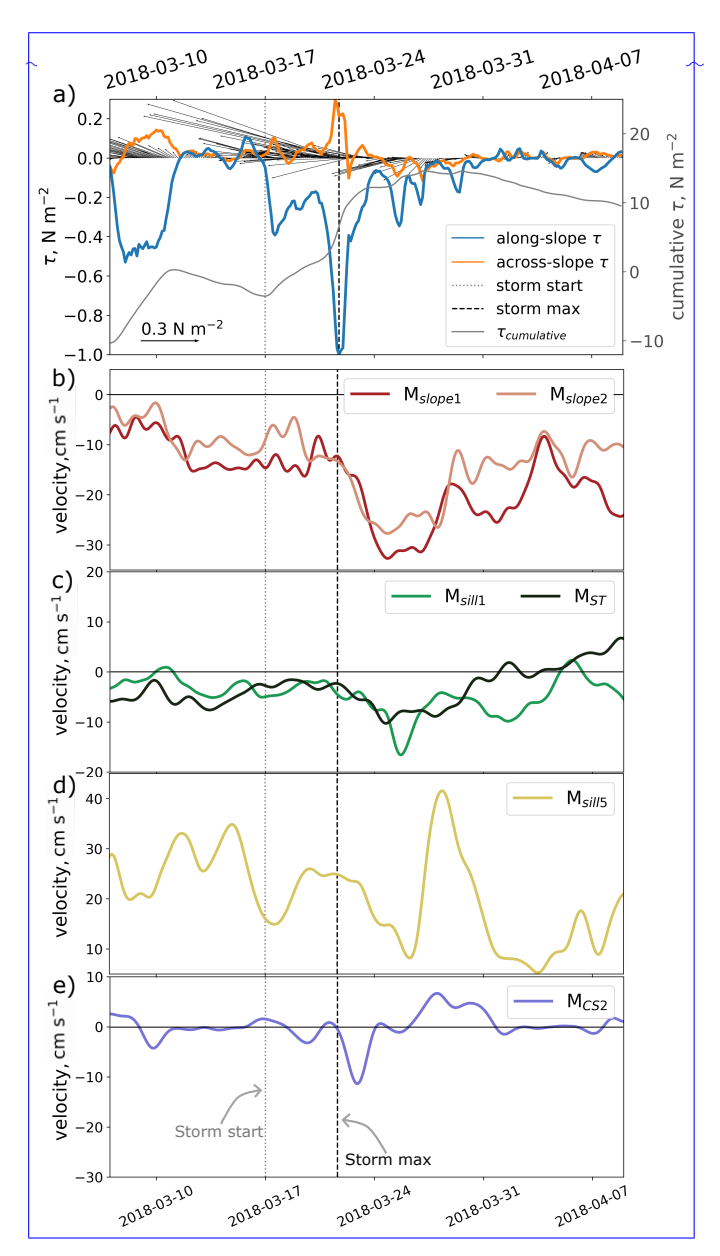


Figure 5. The response to the storm event that started on the 17^{th} of March 2018 (dotted, gray vertical line) and reached maximum ocean surface stress, τ_{max} , on the 22^{th} of March 2018 (dashed, black vertical line). Time series of a) ocean surface stress (τ) averaged over the Upstream box (black sticks), the strength of the along-slope (blue) and cross-slope (orange) components, and the cumulative along-slope τ (gray, de-trended and $180\,\mathrm{day}$ high-pass-filtered). The along-flow current speed at b) M_{slope1} (red) and M_{slope2} (pale red), c) M_{sill1} (green) and M_{ST} (gray), d) M_{sill5} (yellow), and e) the current speed following the bathymetry at M_{CS2} (purple). See Figure 1 for mooring locations.

increase). If we lower the significance threshold from, e.g., the 90^{th} to the 70^{th} percentile, the percentage of storms that are considered to give a significant response at both slope-moorings (M_{slope1} , where we and M_{slope2}) increases from 34% to 66% (Fig. 3). However, we choose to keep our threshold at a conservative value to ensure that we focus on the strongest events with the most notable ocean responses.

We expect the strongest storm response responses at M_{slope1} and M_{slope2} , since they are located over the slope and capture the acceleration of the ASC directly, more than half of the. Here, the mean current speed during the identified response-giving storms is 54% higher than the mean current at M_{slope1} and 50% higher at M_{slope2} (Table 2). Half the storms cause a significant increase in the westward along-flow current (average response: westward $U_{response}$ of response-giving storms: ~ -8 to $-9\,\mathrm{cm}\,\mathrm{s}^{-1}$, Fig. 3, 7e,ea,d, and Table 2). The mean current speed during the response-giving storms is 65% higher than the record mean current at and 42% higher at.

The thermocline over the slopeat, represented by the $-1.7-1.7^{\circ}$ C isotherm, is only weakly pushed down (on average $\sim 30\,\mathrm{m}$ at M_{slope1} and $\sim 40\,\mathrm{m}$ at M_{slope2} during the storms with a significant response at M_{slope1} and M_{slope2} , not shown). This is substantially less than the high-frequency fluctuations in thermocline depth caused by shelf waves and tides (which is on the order of $100-200\,\mathrm{m}$, Semper and Darelius, and thus, depression of the thermocline caused by the storms do does not substantially impede the access of warm water onto the continental shelf. Although the development of a fresh

and warm surface layer has been suggested to

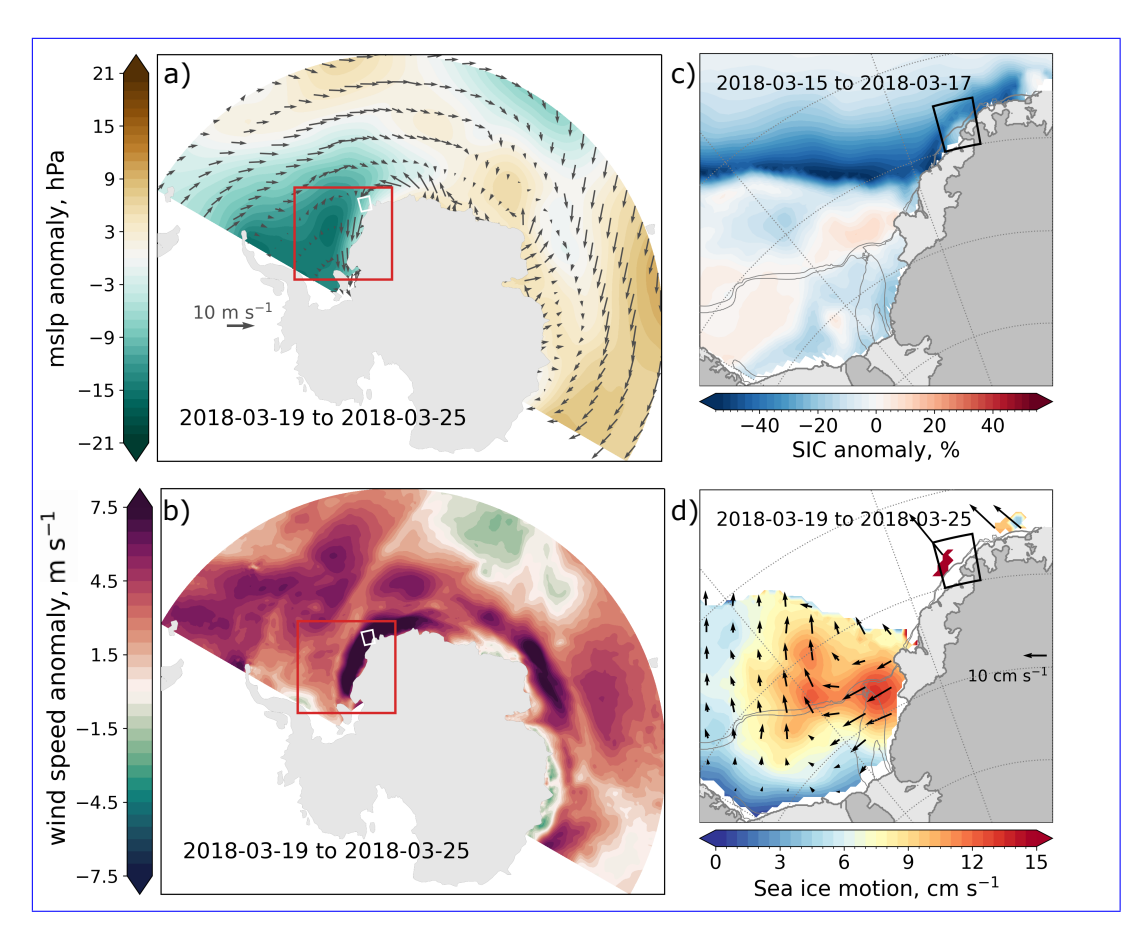


Figure 6. The atmospheric and sea ice conditions during the storm that started on the 17^{th} of March 2018 and reached maximum ocean surface stress, τ_{max} , on the 22^{th} of March. Anomalies of the a) mean sea level pressure with $10\,\mathrm{m}$ wind velocity vectors and b) absolute $10\,\mathrm{m}$ wind speed averaged ± 3 days of τ_{max} relative to the average March field (1990-2023). c) Sea ice concentration averaged over the two days before the storm starts relative to the climatology (past 30 years). d) Sea ice velocity (Tschudi et al., 2019b) averaged ± 3 days of τ_{max} . White regions indicate missing data or areas without sea ice. In a,b), the Upstream box and the region shown in c,d) are indicated, and in c,d), the $1000\,\mathrm{m}$ and $600\,\mathrm{m}$ isobaths are indicated by gray lines (Fretwell et al., 2013). Sea ice concentrations, pressure, and $10\,\mathrm{m}$ wind data are from ERA5 (Hersbach et al., 2023).

Table 2. Overview of parameters from the composite analysis of storm response ($U_{response}$: Equation 5 and Fig. Eq. A1d.5) at the moorings. The % of response-giving storms is estimated relative to the storms occurring during each moorings record.

Mooring	Average anomaly	Response-giving		
name	$U_{response} [{\rm cm \ s^{-1}}]$	storms, N/total		
M_{slope2}	$-11 \pm 6 - 9.1 \pm 6.4$	21 19/ 39 (54 38 (50%)		
$M_{\it slope1}$	$-10 \pm 5 - 8.3 \pm 5.5$	25 21/ 39 (64 38 (55%)		
$M_{\it sill}$	$-8 \pm 4 - 8.7 \pm 5.8$	14 8/ 34 (39 31 (26%)		
\mathbf{M}_{ST}	$\frac{-7 \pm 3}{-8.3 \pm 2.2}$	10 5/ 28 (36 22 (23%)		
$M_{\it sill}$ 5	$16 \pm 10 \cdot 17.0 \pm 9.6$	10 8/ 17 (59 12 (67%)		
${\rm M}_{CS2}$	$\frac{-7 \pm 5}{-6.6 \pm 7.7}$	9 8/ 31 (29 <u>(28</u> %)		

295 may be protected from the wind by the fresh and warm surface layer during summer, as suggested by Daae et al. (2017) and Hattermann (2018).

Both within the inflow on the across the Filchner sill and in the Small Trough (M_{sill1} and M_{ST}) more than one-third roughly 25% of the storms cause a significantly increased southward current significant storm response (average response: and $-8.7\,\mathrm{cm\,s^{-1}}$ and $-8.3\,\mathrm{cm\,s^{-1}}$, Fig. $7_{a,db,e}$, Table 2). At M_{sill1} , all events with a significant response occur between December and June, i.e., from late spring to early winter (Fig. 3)although just 66, although only 57% of all the storms occur during these months (Fig. 4c). The same is true for 80There is also a tendency for a seasonal signal at the slope moorings, where 70% of the events that cause a significant storm response at (Fig. 3), occur in this period.

300

305

310

315

Within the observed ISW outflow, at the location of M_{sill5} , periods of strong along-slope wind co-vary with enhanced overflow on monthly (Daae et al., 2018) time scales time scales (Daae et al., 2018). Idealized numerical experiments (Dundas et al., 2024) also suggest that storms can drive an adjustment of adjust the SSH across a trough, thus connecting the southward inflow and the northward outflow. This is similar to the situation described by Morrison et al. (2020) and observed by Darelius et al. (2023a), where the downslope flow of DSW along a canyon or ridge causes an SSH anomaly that drives an upslope flow of WDW east of the corrugation. We, therefore, expect that the storms-therefore expect the storms to induce enhanced outflow (i.e., northward flow) at M_{sill5} . While the mean current and the high-frequency variability of the outflow at are higher than at the other moorings, the average significant storm response is northward flow at and this is confirmed by the observations (Fig. 7e). c, Table 2).

Just as at the other moorings close to the shelf break, there is a tendency for a seasonal signal in the significant storm response at . Here, 90% of storm responses occur between December and June. This agrees with the seasonality in the observed relationship between wind and the overflow on the sill in 2009 (Daae et al., 2018). We note that the mooring stopped recording current velocities after roughly 1.5 years. Thus, 17 storm periods are captured within this mooring period, which leaves few samples on which to base our conclusions regarding the seasonality in response at . However, this location displays a high fraction of significant storm response events (59% vs. 53% at and , 41% at , and 35% at during the same period, Fig. 3).

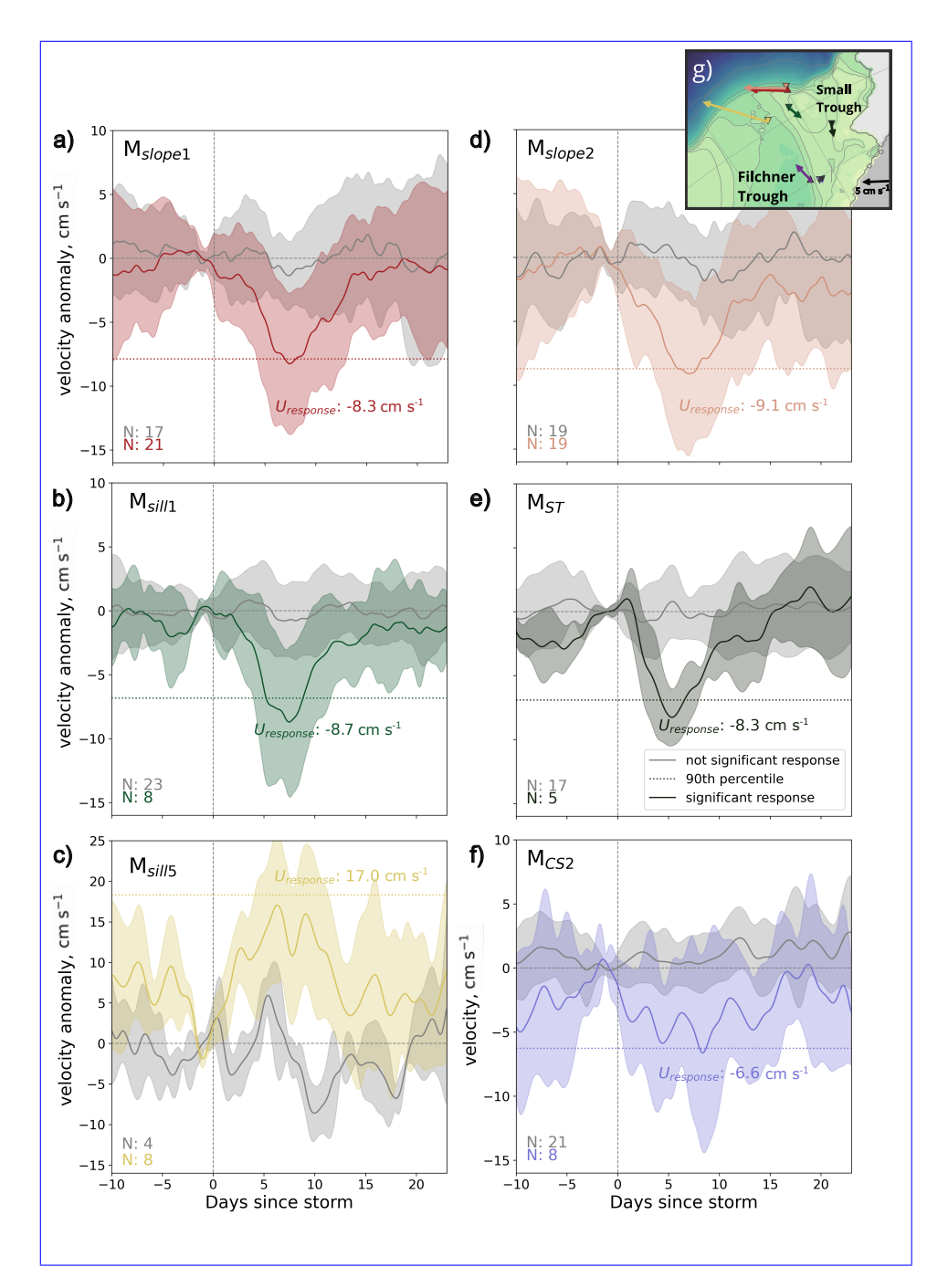


Figure 7. The composite average storm response at a) M_{slope1} , b) M_{sill1} , c) M_{sill5} , d) M_{slope2} , e) M_{ST} , and f) M_{CS2} . In each panel, the average response (line) and the standard deviation (area) to storms that give a significant response (increased velocity anomaly) are shown in color, while the average current following storms that do not give a significant response is shown in gray. The legend in e) is common for all panels. The threshold for significance (see Table 1, horizontal colored, dotted lines) and the number of events (N) included are indicated. Since these composites are estimated individually for each mooring, the specific storms driving the response shown are not always the same (see Fig. 3). Day zero is the start of the period used to estimate $U_{response}$, i.e., $t_0 - 3 \, days$ (see Fig. A1). We only include the events where we have data for the 33 days shown in each panel. Events close to the start or end of each mooring period are consequently not included in this figure. The map in the upper corner (g) shows the mooring locations and their the mean current directions.

The ocean surface stress increase per day is largest in summer and fall Most of the strongest storm events (stress increase rate> $1.5\,\mathrm{N\,m^{-2}\,day^{-1}}$) occur between December and June (Fig. 4). Strong and long storm events are expected to cause the largest current response (Dundas et al., 2024), and thus, the seasonality in storm intensity likely contributes to the (although weak) might contribute to the tendency of seasonality in storm response at M_{sill1} , and The seasonality could also be linked to the seasonal signal in the strength and the baroclinicity of the current at and, which are both strongest during fall and winter (Darelius et al., 2024a). However, we find that the storm response at and does not appear to depend on the baroclinicity prior to the storm (not shown). The M_{ST} . The enhanced current during winter (Darelius et al., 2024a) could, however, also cause a larger current pathway overshoot at the mouth of the trough Filchner Trough opening (Daae et al., 2017), preventing the storm signal from propagating southward along the trough and reaching, and and reaching the mooring locations on the shelf, thus contributing to the tendency of fewer significant storm response events during winter.

At the southernmost mooring location, at M_{CS2} along the eastern flank of Filchner Trough, $\frac{2928\%}{2928\%}$ of the storms cause a significant response (Fig. 3). The average southward flow anomaly during these events is (, average response: $-6.6\,\mathrm{cm\,s^{-1}}$ Fig. 7ef). The fact that significant storm responses are recorded at this location highlights the potential for storms to increase the southward heat transport towards Filchner Ice Shelfin the south. If warm water is present on the continental shelf during a response-giving storm, this warm water will likely be pushed southward as observed by Darelius et al. (2016). However, it will not necessarily reach the mooring during the storm event due to the relatively long background advection time scales (5-9 weeks) from the continental slope to 76° S Steiger et al. (2024)(Steiger et al., 2024).

3.3 Atmospheric Which atmospheric conditions : trigger a storm responseor not?

320

325

330

335

340

345

350

The composite analysis of the eurrent's response to storm events mooring records shows that while many storms drive a significant increase in the current at the various mooring locations, several some storms enhance the circulation, other storms do not. We note, however, that the results are sensitive to our choice of significance threshold. When we lower the threshold for significance from the 90^{th} to the 70^{th} percentile of current increase, the number of storms To investigate the atmospheric conditions that give a significantly enhanced current at both slope-moorings significant storm response we focus on the slope moorings (M_{slope1} and M_{slope2}) increases from 46% to 74% (Fig. $\ref{Fig. Propose2}$ a). At , two storms in 2018 become significant when lowering the threshold (Fig. $\ref{Fig. Propose2}$ a). This emphasizes that the storms we identify as not giving a significant current response may still influence the circulation although we do not resolve this response with our method due to the high background variability.

Most storms that cause a strong since these records are the longest and since most of the storms that induce a response on the Filchner Sill and in the Small Trough also enhance the ASC and show a significant response at the slope moorings give a response on the slope (Fig. 3). Since the records from the slope moorings are the longest, we focus on these when investigating the atmospheric conditions that give a significant storm response.

The response of the ASC We find that an ASC response to a storm depends on the storm duration, the ocean surface stress increase during the storm, and the maximum stress (Fig. 8). We find that Between 2017 and 2021, 70% of storms that are i) longer than four 5.7 days, ii) have a rate of stress increase larger than 0.9 Nm⁻² day⁻¹, and iii) have higher maximum stress

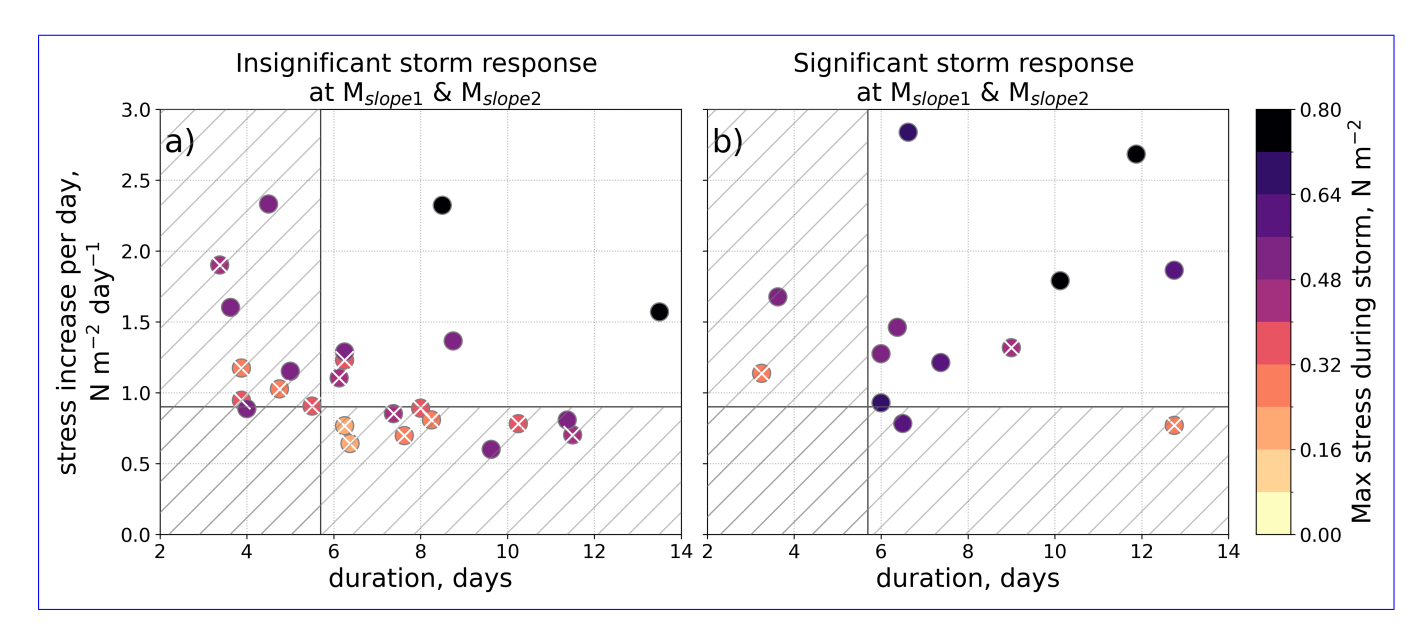


Figure 8. Scatter plots of storm duration and ocean surface stress increase per storm day, colored by the corresponding τ_{max} . The storms that do not induce a significant response at M_{slope2} and M_{slope1} are shown in panel a), and those that do are shown in panel b). The hatched area indicates a duration shorter than four 5.7 days and/or a stress increase smaller than $0.9 \,\mathrm{N\,m^{-2}\,day^{-1}}$. White crosses mark storms with $\tau_{max} < 0.5 \,\mathrm{N\,m^{-2}}$.

than maximum stress higher than $0.5\,\mathrm{N\,m^{-2}}$ over the Upstream box, give a significant increase in the ASC speed during 2017 to 2021. storm response in the slope moorings.

Periods of low ocean surface stress correspond to periods of low variability in the ASC (not shown) and storms occurring during this period are generally without significant storm responses in the ASC. Low ocean surface stress periods generally occur during mid-winter (not shown). We, therefore, hypothesize that the mid-winter sea ice pack dampens the momentum transfer into the ocean. This dampening might be caused by a highly compact sea ice cover (Martin et al., 2014), low rigidity (Steele et al., 1997), low surface and bottom roughness (Martin et al., 2016; Tsamados et al., 2014), or a combination of these factors. When the SIC approaches 100%, the total ocean surface stress is nearly entirely determined by the momentum transfer from the sea ice to the ocean (Eq. 4). Within these periods, the weakest ice-ocean stress is, thus, when the sea ice is the least mobile, which also occurs during mid-winter (not shown). During mid-winter, the mooring locations consequently experience low total ocean surface stress, weak storms (Fig. 4), and weak air-sea momentum transfer. Consequently, there are both few storms (34% of storms, Fig. 4c) between July and November and few (28%) significant storm response events within the ASC (Fig. 3).

Zooming out to

355

360

365

Looking at large-scale atmospheric patterns, the low-pressure systems that give a response at M_{slope1} and M_{slope2} , i.e., significantly enhance the ASC are generally deeper and more structured than those that do not enhance the ASC above the upper part of the continental slope, are deep (Fig. 9a,e,i). The wind speed is strongly average pressure at the center of the

response-giving storms is 968hPa. Both the wind speed and the sea ice movement are thus enhanced along the coast upstream of the study area (Fig. 9b,f,j), and the sea ice movement is high (Fig. 9d,h,ld). Prior to the storm events, the SIC sea ice concentration is also, on average, lower low compared to the climatology when there is a response than when there is not (Fig. 9c). In comparison to these conditions, the conditions during the storms that do not significantly enhance the ASC are less intense. The average pressure at the center of the storms without a response is 978hPa, and the wind speeds and the sea ice movement are lower (Fig. 9e,f,h). The sea ice concentration is also more similar to the climatology (Fig. 9g).

Based on the composites and the case study (Fig. 5), we thus suggest that relatively low sea ice concentration, g, k). We hypothesize that the relatively low SIC, high sea ice mobilityand strongly enhanced, and strong wind along the coast upstream of the southeastern Weddell Sea favor study area are conditions that favor a significant storm response. This is also expected, as these conditions lead to an efficient momentum transfer from the atmosphere into the ocean. This enhances the, enhanced Ekman convergence, and an increased cross-slope SSH and results in overall enhanced ASC and on-shelf circulation. This suggestion is supported by the same patterns occurring during the case study (Fig. 5f-i). SSH-gradient that drives a barotropic response in the ASC.

3.4 A shift in mid-2019

370

375

380

385

390

395

400

At, along the eastern flank of Filehner Trough at 76S, there is an apparent shift in storm response

An apparent change in the storm response occurs during 2019(Fig. ??a), which is most prominent at M_{CS2} : Before July 2019, only one storm event eauses a significant storm response at . After caused a significant response at this location, while after July 2019, 5040% of the storms eause a significant storm caused a significant response (Fig. ??a). Along the slope 3). For the slope moorings, there is a similar, but opposite, tendencytowards but opposite tendency. Here, there are fewer significant storm response events after July 2019 (Fig. ??a3). While we cannot rule this out as out that this is a coincidence, these results indicate that while all locations are susceptible to storm-driven enhanced along-flow currents, i) the potential for a significant storm response appears to depend depends on conditions that vary interannually and ii) a storm response at M_{CS2} is not necessarily driven by an enhanced ASC that then translates propagating from M_{slope1} and M_{slope2} southward along Filchner Trough, i.e., a storm does not necessarily enhance the circulation over the full domain, contrary to suggestions by. The latter is contrary to results from the idealized numerical simulations in Dundas et al. (2024)., where the ASC and the circulation on the shelf east of Filchner Trough were tightly connected. We suggest that the complex bathymetry – and potentially the interplay between the Antarctic Coastal Current and the ASC – are important factors that explain the differences between the results of the idealized model and the observations presented here.

Similar shifts in the response Interannual variability in the sensitivity to wind forcing (correlation on monthly time scales) from one year to another were observed within was also observed in the Antarctic Coastal Current (M_{CC} , mooring location shown in Fig. 1) and on the sill (slightly further east than) by Daae et al. (2018). These shifts were of Filchner Trough (15-day low-pass-filtered, Daae et al., 2018). This variability was associated with shifts in the average wind direction and its strength along the coast upstream of Filchner Trough: When the wind had a northwestward component and the windspeed wind speed was low, correlation with the the correlation between the wind and the current weakened. We do not observe a

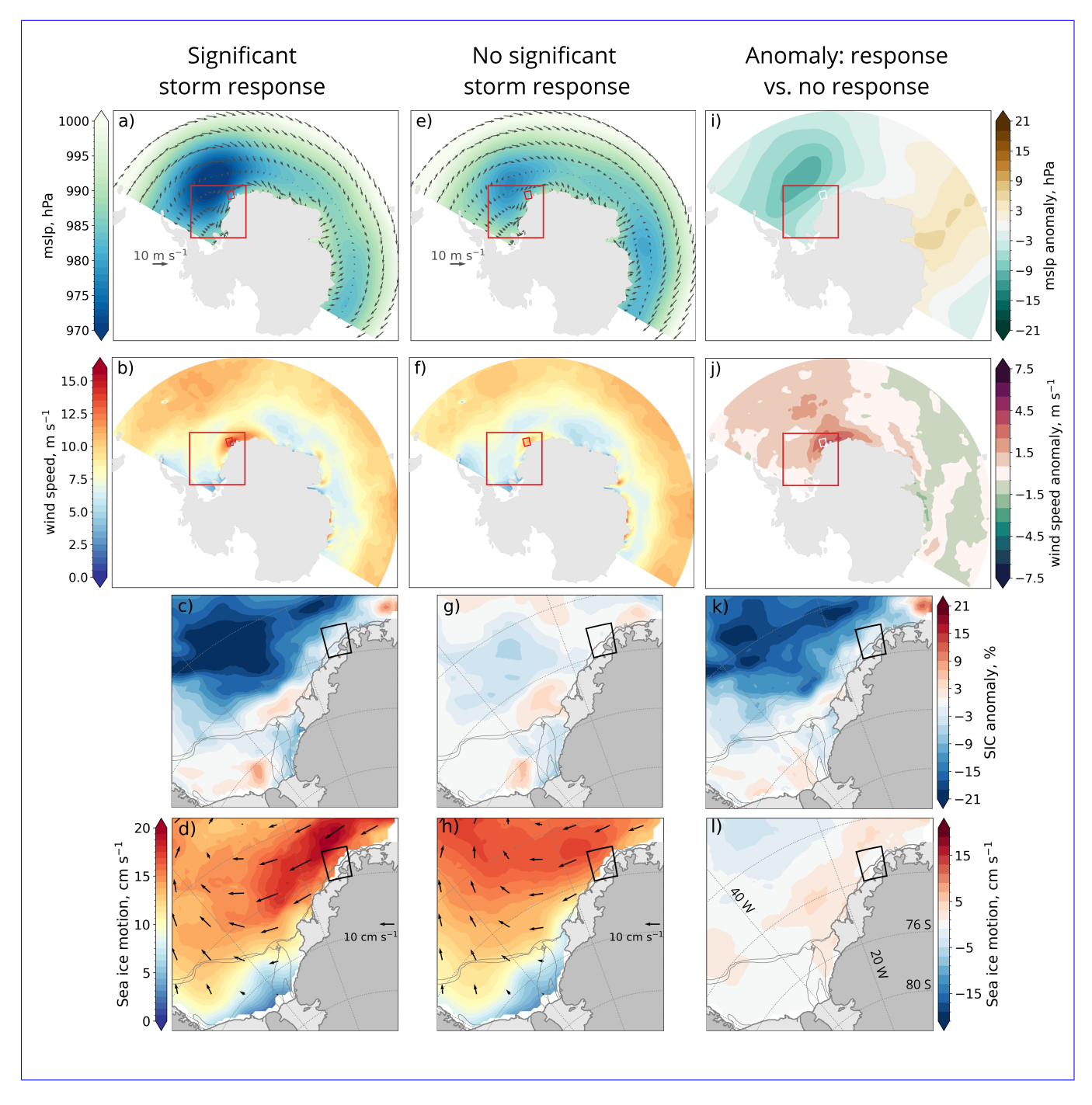


Figure 9. Composite mean atmospheric fields during storms a-d) with and e-h) without a significant storm response at M_{slope1} and M_{slope2} . The difference between the fields during storms with and without a response is shown in i-l). The first row shows the mean sea level pressure (color) and the mean $10 \,\mathrm{m}$ wind (grey gray arrows) $\pm 3 \,\mathrm{days}$ of τ_{max} . The second row shows the wind speed in color and is otherwise equal to row one. The third row shows the mean SIC-sea ice concentration anomaly (with seasonal climatology removed) in a two-day-long two-day window ending when the storm starts begins. The fourth row shows the speed of the sea ice motion (color) and its velocity (black arrows) in a six-day-long window centered at $\pm 3 \,\mathrm{days}$ of τ_{max} . White regions $20 \,\mathrm{max}$ without sea ice.

substantial change in the direction of the mean ocean surface stress before and after mid-2019 (not shown), and while there is a reduction in the variability and average speed strength of the zonal stress, these changes are small-minor (Fig. B1a).

Since there e). There is neither an apparent change in the strength nor in the duration of the storms (Fig. 3 and 4) in July 2019, we investigate if the shift during 2019 might be caused by a change in background circulation or 4 and 3).

We do, however, identify several changes in the background circulation and hydrography on the shelf. We note that after during 2019 (Fig. B1). After July 2019 i) the current at M_{CS2} veers eastward (Fig. ??bB1f), ii) the correlation between the along-coast wind and the southward along-isobath current at M_{CS2} shifts from negative to positive, where a positive correlation indicates that a southwestward wind corresponds to a southward current (Fig. ??echanges sign (Fig. B1a), iii) ISW starts to dominate the winter hydrography at M_{CS2} and is associated with increased variability in the current (Fig. B1b), iv). Additionally, we note that iv) a transition from "Berkner mode" to "Ronne mode" occurred in mid-2018 (Hattermann et al., 2021; Janout et al., 2021), v) at the shelf break, the warmest water is anomalously warm after mid-2019 and the seasonal cycle is disrupted (Darelius et al., 2023b), and vafter mid-2019 (Darelius et al., 2023b) and that, vi) the summertime SIC increases sea ice concentration increases in 2019 (Steiger et al., 2024).

It is beyond the scope of the present study to investigate the relationship between these changes and the apparent shift in the regional storm response. We note, however, that changes in the summer sea ice cover are likely to play a role, as it agrees with the results of the composite analysis that low sea ice concentration favors significant storm responses in the ASC. A more detailed presentation and discussion of the changes occurring in 2019 is found in Appendix B.

4 Conclusions

405

We analyze a network of moorings and confirm that storms can enhance the circulation on the southeastern Weddell Sea continental shelf. These events do not have a systematic significant ocean current response but when they do, they clearly strengthen the westward Antarctic Slope Current (ASC), the dense outflow from Filchner Trough, the southward flow along the eastern flank of Filchner Trough, and the inflow through the Small Trough. Our findings provide observational evidence that storms can enhance the southward transport of warm water towards the Filchner Ice front, as suggested by Darelius et al. (2016) and by the numerical experiments of Dundas et al. (2024).

The duration of a storm, the total cumulated ocean surface stress during the event, and the maximum stress, will, to a large extent, determine whether a storm event enhances the ASC: 70% of the observed storms that are longer than 5.7 days, have a larger stress increase than $0.9 \,\mathrm{N\,m^{-2}\,day^{-1}}$, and $\tau_{max} > 0.5 \,\mathrm{N\,m^{-2}}$, give a significant increase in the ASC.

The interannual variability in the storm response – notably the apparent shift in 2019 that we are unable to explain – highlights the importance of ambient conditions in determining the response of the ASC and the currents on the continental shelf to wind forcing. It also points to a knowledge gap that needs to be addressed if we are to predict how the system evolves in a future of climate change.

Longer observational time series from the region, in combination with designated experiments in a regional model setup, would help us to further understand the observed variability in storm response. A regional model could also provide estimates

of the storm-driven heat transport across the shelf and its importance relative to the heat transport driven by the background flow. The present study, however, provides evidence that storms along the coast upstream of Filchner Trough can enhance the circulation on the shelf, potentially allowing heat to reach the ice front before it is lost to the atmosphere through wintertime convection.

Data availability. The mooring data are, or will be, publicly available. M_{slope1} is available at Darelius et al. (2024), M_{slope2} at Darelius et al. (2023), M_{CS2} and M_{CS3} at Janout et al. (2022), and M_{ST} and M_{sill1} at Steiger and J.-B. (2023). M_{sill5} will be available at NMDC (Østerhus, 2024). The atmospheric data and sea ice concentration from ERA5 reanalysis (Hersbach et al., 2019) is available at Hersbach et al. (2023), the sea ice movement data from NSIDC is available at Tschudi et al. (2019a), and the data of bathymetry, ice shelves, and ice sheets from bedmap2 (Fretwell et al., 2013) is available at Fretwell et al. (2022). Bedmap2 is used in all maps except in Fig. 6a,b), the upper two rows of Fig. 9 and Fig. A2, where the coastlines are drawn using cartopy's "coastline" functionality.

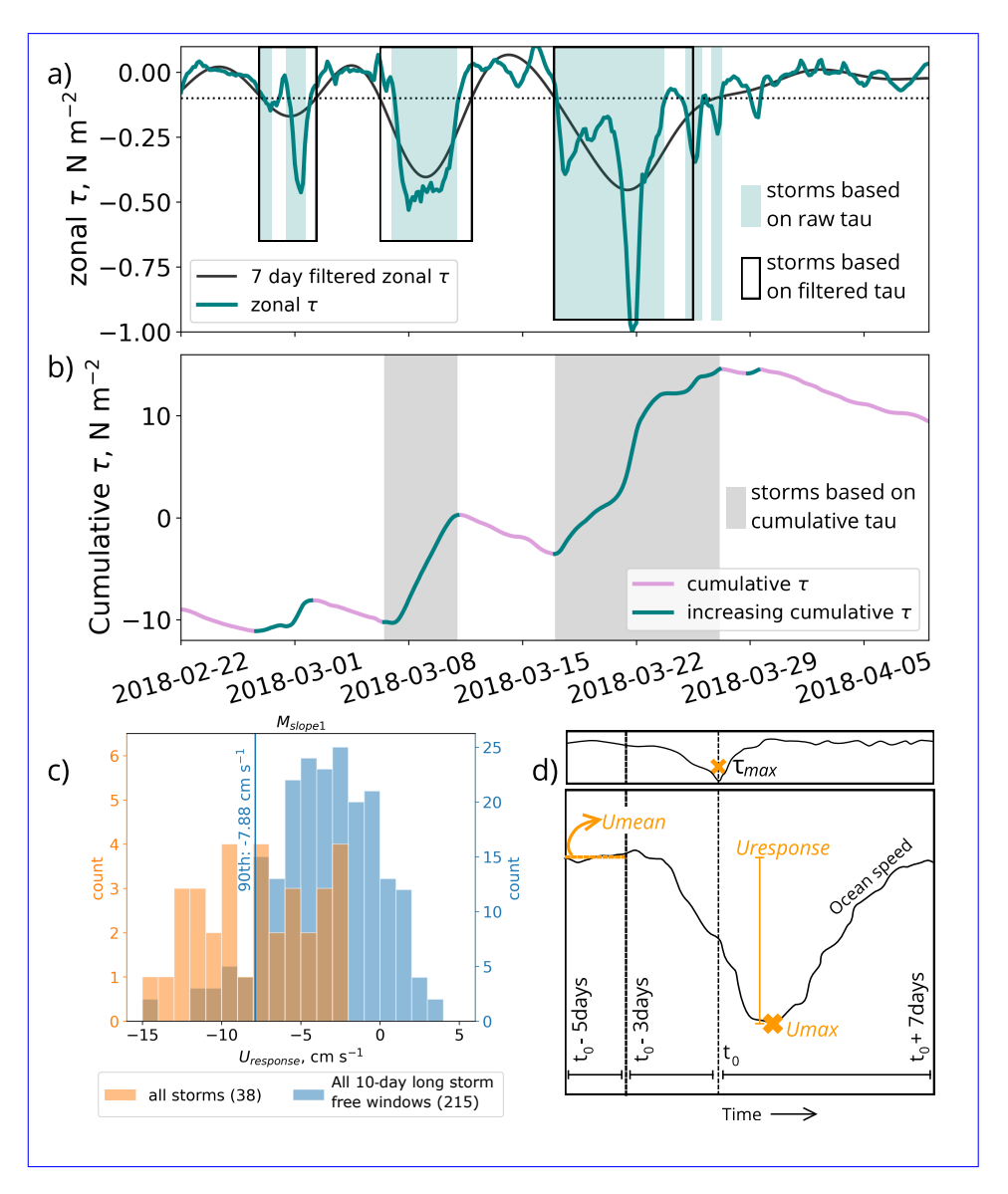


Figure A1. a,b) Example of the storm detection algorithm described in section 2.3. Time series of a) eastward ocean surface stress and b) the cumulative westward ocean surface stress. Identified storm periods are indicated based on a) the raw ocean surface stress (blue shading) and lowpass filtered ocean surface stress (black boxes) and b) based on cumulative ocean surface stress (gray shading), which we use throughout our analysis. c,d) Illustrate the procedures used to determine significance and to identify $U_{Tesponse}$ as described in section 2.5. c) Histogram of $U_{Tesponse}$ (orange) and the current increase during all 10-day long storm-free windows (blue) at M_{slope1} . The 90^{th} percentile, which is used to determine significance, is indicated (blue line). d) A sketch of the procedure used to identify $U_{Tesponse}$, indicating the definition of T_{Thagg} in the upper sub-panel and $U_{Tesponse}$, and $U_{Tesponse}$ in the lower sub-panel.

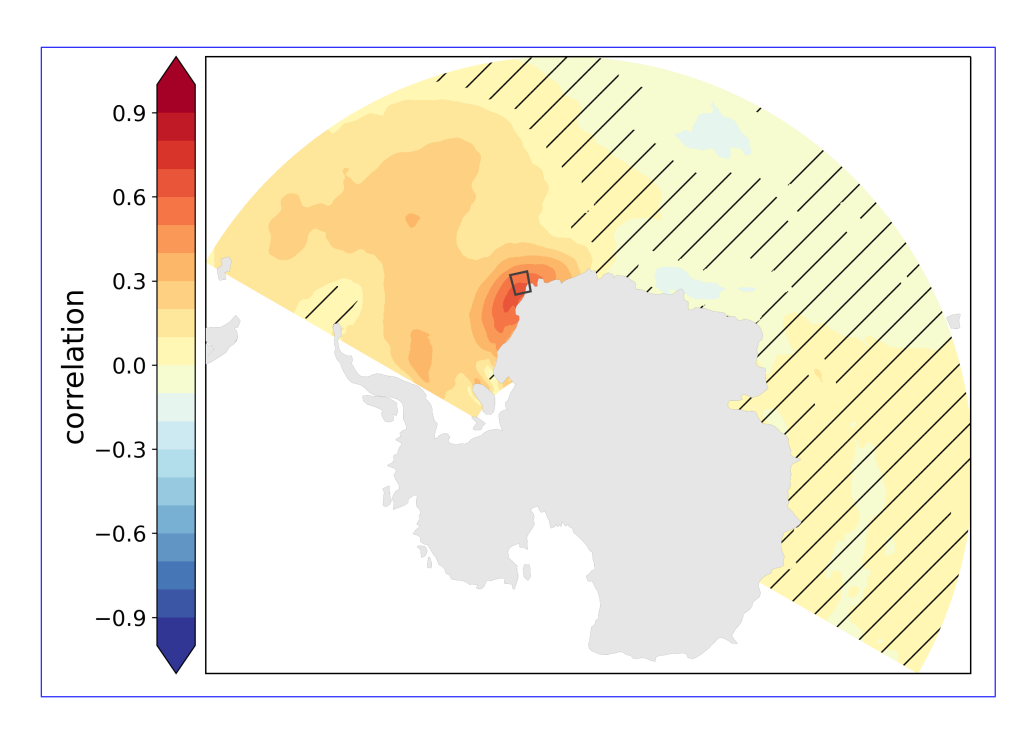


Figure A2. Correlation map of the average wind speed in the Upstream box (black rectangle) vs. the overall wind field during the observation period (2017-2021). Hatched regions indicate insignificant correlation at the 0.95 significance level.

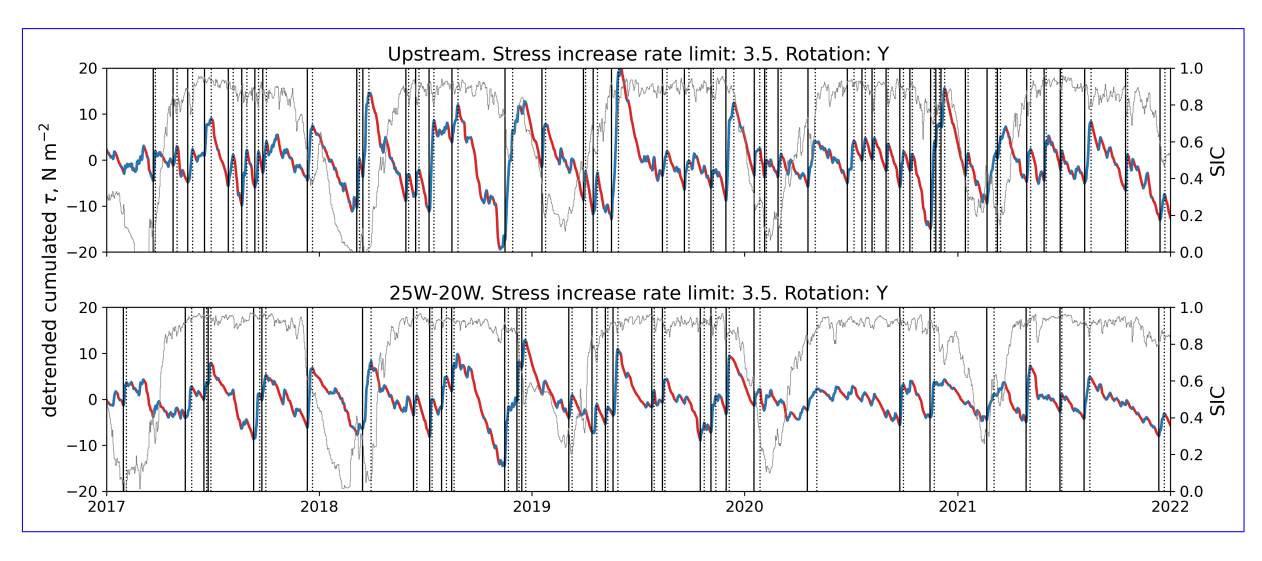


Figure A3. Time series of cumulative and detrended ocean surface stress over the upstream box (upper panel) and a region further west (25°W to 20°W) to indicate the difference in storm identification. Solid black lines indicate storm start and dashed lines are the storm end. The blue parts of the curve highlight increasing cumulative ocean surface stress while the red parts are decreasing.

Appendix B: Changes during 2019 and possible connections to oceanic storm response

450

455

460

465

470

The consistent eastward direction of the current at M_{CS2} from 2019 and onwards (Fig. ??bB1f) is in stark contrast to the current at this location from 2014 to 2016: Thenthen, the current had a strong seasonal cycle with a southwestward eurrent direction during the warm season and west or northward during the cold season (Ryan et al., 2017). We speculate that the interannual variability in storm response might may be related to changes in background circulation at the location. This could be driven by variable interaction between the southward current along the eastern flank of Filchner Trough, the inflow through the Small Trough, and the Coastal Current as they all interact where the zonal extent of the on the narrow continental shelf east of Filchner Trough shrinksat roughly 76°S. The complex bathymetry in the region of M_{CS2} might thus play an important role in impeding hinder the southward signal from propagating neatly southward as it does in the model setup with idealized geometry (Dundas et al., 2024).

Since the 2019 shift is not only local-locally present at 76°S but also appears to affect in the storm response on the slope, it is possible that properties of the Antarctic Coastal Current (M_{CC} , Fig. 1) might affect the shift. Daae et al. (2018) observe a shift in the correlation between wind and the currents (on monthly time scales) at moorings from the Filchner Sill and the Coastal Current (M_{CC}) between 2003 and 2004 (locations indicated in Fig. 1). The Coastal Current (on the shelf) had the strongest correlation with the wind in 2003, and while the outflow at the sill showed the highest correlation in 2004 (Daae et al., 2018). This shift is hence similar to the shift in storm response we observed in 2019: the storm response on the shelf increases when the storm response on the slope decreases. One possible explanation could be that the storm-enhanced signal under certain conditions propagates mainly along the shelf break, causing a strong signal at the slope moorings, and in other not yet identified conditions, mainly propagates along the coast, causing a strong signal at the M_{CS2} mooring. In such a scenario, we would, however, also expect a stronger storm-response at a mooring located just east of M_{CS2} from mid-2019 onwards, but this is not the case (not shown).

Indications of a shift around 2019 in the southeastern Weddell Sea shelf region. Panels a) and c) have a shared x-axis, the purple background indicates the period after July 2019, and the vertical purple dashed line indicates the 1st of July 2019. Panel a) is a simplified version of Fig. 3 showing only moorings and (red) and (purple). The dark bars indicate significant storm responses, and the light bars show storm responses stronger than the 70^{th} percentile of background current increase (see methods 2.5). Panel b) is a progressive vector diagram of the current at the bottom sensor of colored by temperature. The temperature is based on θ and not Θ because the salinity sensor stopped recording in early 2020. The start of the time series (star) and the 1st of July 2019 (dashed line) are indicated. c) Time series from of 90-day long, 33% overlapping windows of significant correlation (black bars) between the along-coast wind and the southward bottom current.

In mid-2018, the circulation under the northern section of Filchner Ice Shelf changed from "Berkner mode" to "Ronne mode" (Hattermann et al., 2021; Janout et al., 2021). This means that the source waters of the ISW observed in the Filchner cavity originated from the Ronne Trough after 2018 rather than from the Berkner Shelf. We considered the possibility that the mid-2019 shift in storm response at the M_{CS2} location could be a delayed response (roughly one year lag) to this large-scale shift in circulation and hydrography. However, at M_{CS3} , which captures the northward-flowing ISW leaving the cavity, indications

of the change from Berkner to Ronne mode appear already in 2018. Following the start of 2019, Ronne-sourced ISW is already consistently present at 76°S and the current has veered eastward (Fig. B1c,d). It, therefore, seems unlikely that f). Due to this offset in timing between the shift in hydrography and circulation due to the shift following the transition from Berkner to Ronne mode is a direct driver of and the shift in storm-response potential at storm response along the continental slope (M_{slope1} and M_{slope2}) and in Filchner Trough (M_{CS2}), we are hesitant to suggest a direct link between the events. What causes the interannual shift in storm response in the southeastern Weddell Sea thus remains an open question.

We analyze a network of moorings and confirm that sudden strong ocean surface stress events – "storms" – can enhance the circulation on the southeastern Weddell Sea continental shelf. These events strengthen the westward Antarctic Slope Current (ASC), the dense outflow from the Filchner Trough,

Appendix C: Source salinity estimates

505

510

To estimate the arrival of the southward flow along the eastern flank of the Filchner Trough, and the inflow through the Small Trough. These observations thus support the suggestions by Darelius et al. (2016) and the numerical experiments of Dundas et al. (2024). Our findings provide observational evidence that storms impact the southward transport of warm water in this region and suggest that this signal may extend beyond 76S, potentially reaching the front of the Filchner Ice Shelf (Darelius et al., 2016). Since storms have the potential to enhance the southward current on the shelf, they also have the potential to push warm water southward whenever warm water is present along the eastern flank of Filchner Trough or in the Small Trough. We suggest that this is also true whenever warm water is present on the continental shelf east of Filchner Trough. shift from Berkner to Ronne mode described by Hattermann et al. (2021) and Janout et al. (2021), we estimate the source salinity of the waters whose temperature and salinity are measured at M_{CS3} by identifying the intersection between the Gade line (Gade, 1979) and the surface freezing point in ΘS_A space (illustrated in Fig. C1). Solving the linear relationship given by Wåhlin et al. (2010) for the source salinity, S₀, gives

$$S_0 = S \left[1 + \frac{cp}{L_f} (T_0 - T) \right],\tag{C1}$$

The duration of a storm, the total cumulated ocean surface stress during the event, and the maximum stress, will, to a large extent, determine whether a storm event will cause a response in the current or not. The response is, as expected, particularly elear in the moorings on the upper part of the slope, i.e., within the ASC. 70% of the observed storms that are longer than four days, have a larger stress increase than , and τ_{max} >, give a significant increase in the ASC. where $cp = 4186 \text{ J kg}^{-1} \text{ K}^{-1}$ is the specific heat capacity of sea water and $L_f = 3.34 \times 10^5 \text{ J kg}^{-1}$ is the latent heat of fusion. By first estimating the surface freezing temperature, T_0 , at the recorded salinity, S_0 , and then using Eq. C1 to estimate the corresponding source salinity, S_0 , we obtain an initial estimate of where the salinity-dependent surface freezing point intersects with the Gade line. The calculation is repeated once, replacing S by S_0 to find a new T_0 and S_0 (Fig. C1).

The enhanced circulation is, however, not so structured and steady that it can consistently be followed neatly from moorings on the slope via the sill to moorings on the shelf at 76S. While some storms enhance the circulation in the whole region, not all

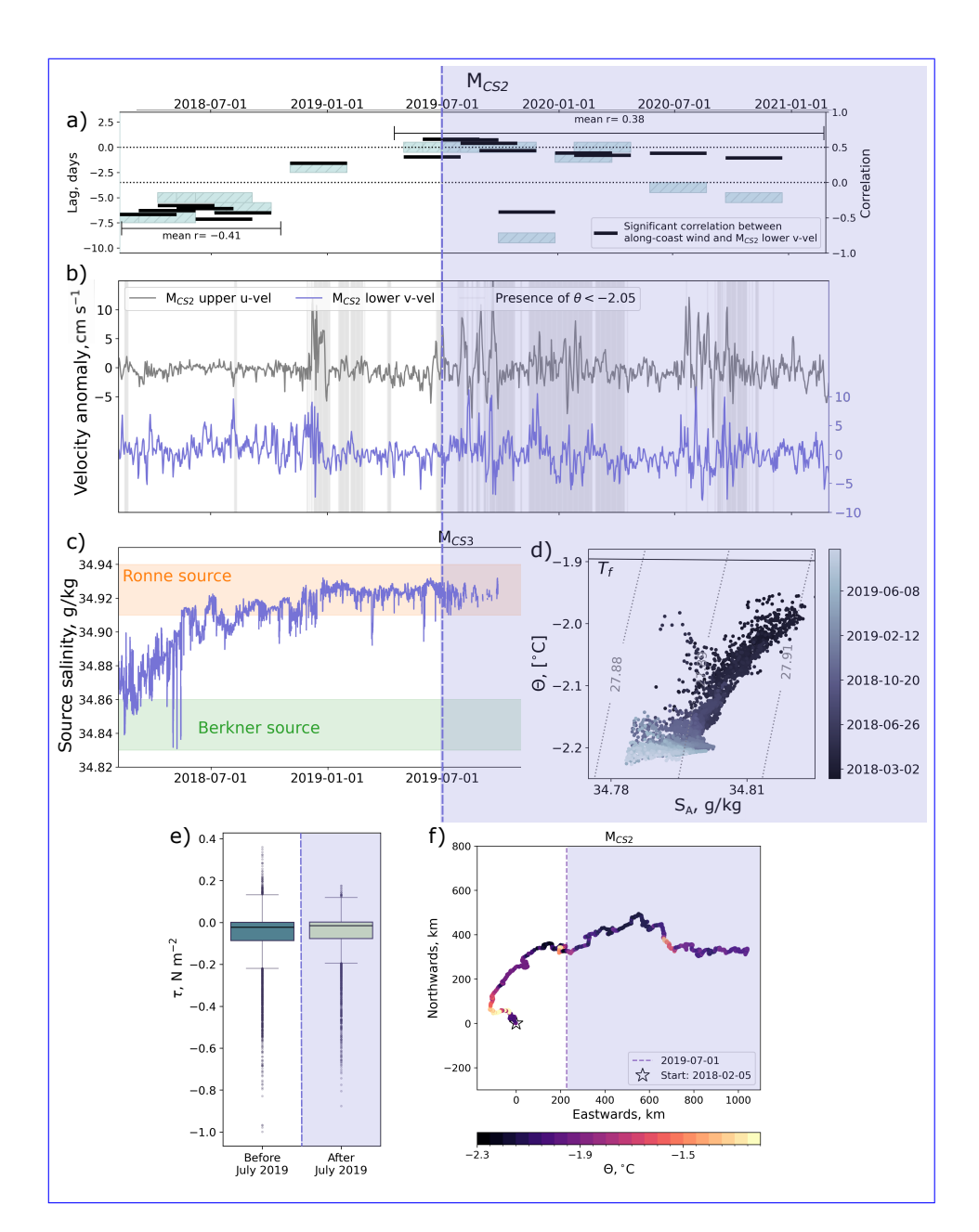


Figure B1. Indications of a shift around 2019 in the southeastern Weddell Sea shelf region. Panels a-c) have a shared x-axis, the purple background indicates the period after 1st of July 2019. a) Time series from M_{CS2} of 90-day long, 33% overlapping windows of significant correlation (black bars) and lag (blue bars) between the along-coast wind and the southward bottom current (24h-30 days bandpass filtered. Positive correlation: roughly south-westward wind corresponds to current toward Filchner Ice Shelf). b) Current anomalies at M_{CS2} ; eastward component at the upper sensor (gray) and the northward component at the lower sensor (purple) with gray shading when water colder than θ =-2.05°C is present. c) The estimated ISW source water salinity at M_{CS3} with approximate ranges of Berkner (green shading) and Ronne (orange shading) mode source waters (Hattermann et al., 2021). d) ΘS_A -diagram from M_{CS3} colored by time. For clarity, we have omitted observations with σ <27.885 kg m⁻³ in panels c) and d). e) Box plots of the along-slope ocean surface stress before (blue) and after (green) July 2019. f) Progressive vector diagram of the current at the bottom gensor of M_{CS2} colored by temperature. The temperature is based on the average absolute salinity (at the nearest sensor level) because the salinity sensor stopped recording in early 2020. The start of the time series (star) and the 1st of July 2019 (dashed line) are indicated.

storm events cause such a consistent response. This differs from the results of an idealized model Dundas et al. (2024), where storm events initiated an overall cyclonic circulation over the continental shelf east of Filchner Trough. We suggest that the complex bathymetry – and potentially the interplay between the Antarctic Coastal Current and the ASC – are important factors that explain the differences between the results of the idealized model and the observations presented here.

The cause of the shift during winter 2019 from conditions that favor a storm response in the ASC to conditions that favor a storm response on the shelf at 76°S remains an open question. Other properties change around the same time, such as warmer temperatures along the slope (Darelius et al., 2023b), a shift from negative to positive correlation between the along-shore south-westward wind and the southward current, and a shift from low to high variability in the current itself at 76°S. Following the start of 2019, Ronne-sourced ISW is consistently present at 76°S. This change is related to an overall shift from Berkner mode to Ronne mode (Hattermann et al., 2021; Janout et al., 2021) and co-occurs with a shift in the current direction at 76°S. However, as the timing of these shifts is offset by roughly half a year, we are hesitant to suggest a link between the events. These inter-annual shifts in atmospheric forcing, hydrography, and circulation emphasize the importance of background conditions for the potential effect of storms in the southeastern Weddell Sea.

The up to four-year-long mooring records analyzed here give clear indications of the effect of storms on the ocean circulation in the Filchner Trough region, however, longer observational time series at the mooring sites or experiments run in a regional model setup would be helpful to understand the observed variability in storm response. Based on the results presented here, a regional model could also enable a realistic estimate of the potential heat transport at the ice front driven by the storm events and its importance relative to the heat transport driven by the background flow. While this would yield additional information about the importance of storms for the basal melt of the Filchner Ice Shelf, the present study confirms the ability of storms to enhance circulation, which is the basis for bringing warm water southward towards Filchner Ronne Ice Shelf.

Appendix D: Supporting figures

515

520

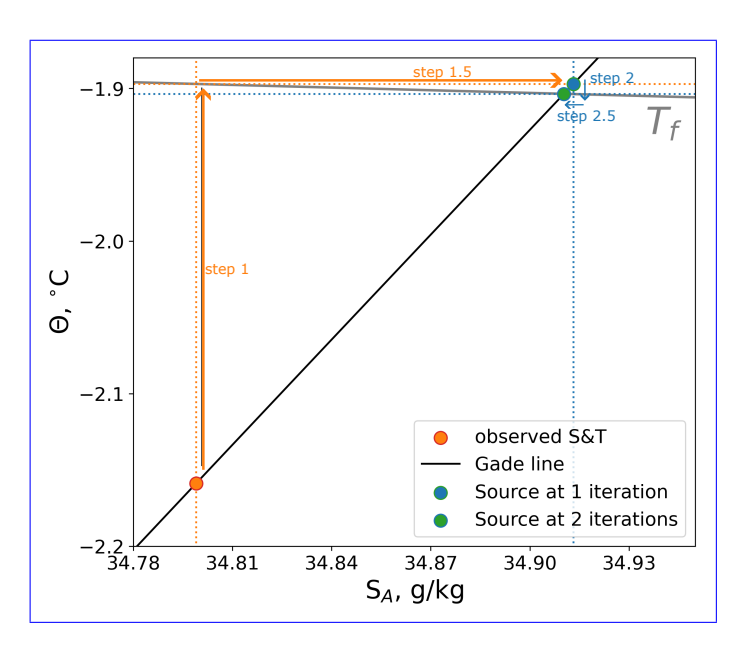


Figure C1. Correlation map—Illustration of the average wind speed in method to estimate source salinity following Equation C1. The desired value is the Upstream box temperature and salinity at the intersection between the relevant Gade line (black rectangleline) vsand the salinity-dependent freezing point (gray line). The process is as follows: given an observed temperature and salinity pair (orange dot), the overall wind field during the observation period freezing point is estimated (2017-2021step 1). Hatched regions indicate insignificant correlation. Then, the salinity at this temperature of the 0.95 significance level Gade line is estimated (step 1.5). This completes iteration 1 and the first approximation of the source temperature and salinity (blue dot). Completing one more iteration (steps 2 and 2.5) gives a good approximation of the source water properties (green dot).

Example of the storm detection algorithm a,b) described in section 2.3. Time series of a) eastward ocean surface stress and b) the eumulative westward ocean surface stress. Identified storm periods based on a) the raw ocean surface stress (blue shading) and lowpass filtered ocean surface stress (black boxes) and b) based on cumulative ocean surface stress, which is the algorithm we use throughout our analysis (gray shading) are indicated, e,d) Illustrate the procedures used to determine significance and to identify $U_{response}$ as described in section 2.5. c) Histogram of $U_{response}$ (orange) and the current increase during all 10-day long storm-free windows (blue) at . The 90th percentile, which is used to determine significance, is indicated (black line). d) A sketch of the procedure used to identify $U_{response}$; indicating the definition of τ_{max} in the upper sub-panel and U_{mean} , U_{max} , and $U_{response}$ in the lower sub-panel.

Additional indications of a shift around 2019 in the southeastern Weddell Sea shelf region following the same setup as Fig. ??: The purple background indicates the period after July 2019, and the vertical purple dashed line indicates the 1st of July 2019. Panel a) shows box plots of the zonal ocean surface stress before (blue) and after (green) July 2019. Panels b) and c) have a shared x-axis. b) Time series from of current anomalies; eastward component at the upper sensor (gray) and the northward component at the lower sensor (purple). The gray shading indicates approximate ranges of Berkner (green) and Ronne (orange) mode source waters (Hattermann et al., 2021). d) ΘS_A -diagram from colored by time, with darker colors at the start of the record. For clarity, we have omitted observations with σ <in panels e) and d).

Illustration of the method to estimate source salinity following Equation C1. The desired value is the temperature and salinity at the intersection between the relevant Gade line and the salinity-dependent freezing point (green dot). The process is as follows: given an observed temperature and salinity pair (orange dot), the freezing point is estimated (step 1). Then, the salinity at this temperature of the Gade line is estimated (step 1.5). This completes iteration 1 and the first approximation of the source temperature and salinity (blue dot). Completing one more iteration (steps 2 and 2.5) gives a good approximation of the source water properties (green dot).

Author contributions. VD analyzed the mooring and atmospheric data, prepared the figures, and drafted the paper under the supervision of KD and ED. MJ prepared the data from the M_{CS2} and M_{CS3} moorings, JBS prepared the data from the M_{sill1} and M_{ST} moorings, SØ prepared the data from the M_{sill5} mooring, and ED prepared the data from the M_{slope1} and M_{slope2} moorings. All the co-authors read and contributed to the text and the discussion.

Competing interests. The contact author has declared that none of the authors has any competing interests.

540

Acknowledgements. We would like to thank Keith Nicholls, Angelica Renner, and one anonymous reviewer for valuable input and comments on this manuscript. This work was funded through the Norwegian Research Council, project numbers 267660 and 328941, and uses samples and data provided by the Alfred Wegener Institute Helmholtz-Center for Polar- and Marine Research in Bremerhaven (Grant No. AWI-PS124-03) and the European Union's Horizon 2020 research and innovation program under grant agreement N°821001 (SO-CHIC), N°820575 (TiPACCs), and N°101060452 (OCEAN:ICE). The moorings were recovered during the COSMUS expedition (PS124), and we would like to extend thanks to the officers and crew of the RV Polarstern for their work on the COSMUS cruise PS124.

References

560

565

570

- Arthun, M., Nicholls, K. W., Makinson, K., Fedak, M. A., and Boehme, L.: Seasonal inflow of warm water onto the southern Weddell Sea continental shelf. Antarctica. Geophysical Research Letters. 39, 2–7, https://doi.org/10.1029/2012GL052856, 2012.
 - Caton Harrison, T., Biri, S., Bracegirdle, T. J., King, J. C., Kent, E. C., Vignon, E., and Turner, J.: Reanalysis representation of low-level winds in the Antarctic near-coastal region, Weather and Climate Dynamics, 3, 1415–1437, https://doi.org/10.5194/wcd-3-1415-2022, 2022.
- Daae, K., Hattermann, T., Darelius, E., and Fer, I.: On the effect of topography and wind on warm water inflow—An ideal-ized study of the southern Weddell Sea continental shelf system, Journal of Geophysical Research: Oceans, 122, 2622–2641, https://doi.org/10.1002/2016JC012541, 2017.
 - Daae, K., Darelius, E., Fer, I., Østerhus, S., and Ryan, S.: Wind stress mediated variability of the Filchner trough Overflow, Weddell sea, Journal of Geophysical Research: Oceans, 123, 3186–3203, https://doi.org/10.1002/2017JC013579, 2018.
- Daae, K., Hattermann, T., Darelius, E., Mueller, R. D., Naughten, K. A., Timmermann, R., and Hellmer, H. H.: Necessary Conditions for Warm Inflow Toward the Filchner Ice Shelf, Weddell Sea, Geophysical Research Letters, 47, https://doi.org/10.1029/2020GL089237, 2020.
 - Darelius, E., Makinson, K., Daae, K., Fer, I., Holland, P. R., and Nicholls, K. W.: Hydrography and circulation in the Filchner Depression, Weddell Sea, Antarctica, Journal of Geophysical Research C: Oceans, 119, 5797–5814, https://doi.org/10.1002/2014JC010225, 2014.
 - Darelius, E., Fer, I., and Nicholls, K. W.: Observed vulnerability of Filchner-Ronne Ice Shelf to wind-driven inflow of warm deep water, Nature Publishing Group, pp. 1–7, https://doi.org/10.1038/ncomms12300, 2016.
 - Darelius, E., Daae, K., Dundas, V., Fer, I., Hellmer, H. H., Janout, M., Nicholls, K. W., Sallée, J. B., and Østerhus, S.: Observational evidence for on-shelf heat transport driven by dense water export in the Weddell Sea, Nature Communications, 14, https://doi.org/10.1038/s41467-023-36580-3, 2023a.
 - Darelius, E., Dundas, V., Janout, M., and Tippenhauer, S.: Sudden, local temperature increase above the continental slope in the southern Weddell Sea, Antarctica, Ocean Science, 19, 671–683, https://doi.org/10.5194/os-19-671-2023, 2023b.
 - Darelius, E., Janout, M. A., Fer, I., and Sallée, J.-B.: Physical oceanography and current velocity data from mooring M3 on the upper continental slope, east of Filchner Trough, February 2017 February 2021, https://doi.org/10.1594/PANGAEA.962043, 2023.
 - Darelius, E., Fer, I., Janout, M., Daae, K., and Steiger, N.: Observations of the Antarctic Slope Current in the Southeast-ern Weddell Sea: A Bottom-Enhanced Current and Its Seasonal Variability, Journal of Geophysical Research: Oceans, 129, https://doi.org/10.1029/2023JC020666, 2024a.
 - Darelius, E., Fer, I., Janout, M. A., Daae, K., and Steiger, N.: Observations of the Antarctic Slope Current in the southeastern Weddell Sea: a bottom-enhanced current and its seasonal variability, Journal of Geophysical Research: Oceans, https://doi.org/10.1029/2023JC020666, 2024b.
- Darelius, E., Janout, M. A., Fer, I., and Sallée, J.-B.: Physical oceanography and current velocity data from mooring M6 on the upper continental slope, east of Filchner Trough, February 2017 February 2021, https://doi.org/10.1594/PANGAEA.964715, 2024.
 - Dotto, T. S., Naveira Garabato, A., Bacon, S., Tsamados, M., Holland, P. R., Hooley, J., Frajka-Williams, E., Ridout, A., and Meredith, M. P.: Variability of the Ross Gyre, Southern Ocean: Drivers and Responses Revealed by Satellite Altimetry, Geophysical Research Letters, 45, 6195–6204, https://doi.org/10.1029/2018GL078607, 2018.

- Dundas, V., Daae, K., and Darelius, E.: Storm-Driven Warm Inflow Toward Ice Shelf Cavities—An Idealized Study of the Southern Weddell Sea Continental Shelf System, Journal of Geophysical Research: Oceans, 129, https://doi.org/https://doi.org/10.1029/2023JC020749, 2024.
 - Foldvik, A., Gammelsrød, T., and Tørresen, T.: Hydrographic observations from the Weddell Sea during the Norwegian Antarctic Research Expedition 1976/77, Polar Research 3, pp. 177–193, 1985.
- Foldvik, A., Gammelsrød, T., Øterhus, S., Fahrbach, E., Rohardt, G., Schröder, M., Nicholls, K. W., Padman, L., and Woodgate, R. A.:

 Ice shelf water overflow and bottom water formation in the southern Weddell Sea, Journal of Geophysical Research: Oceans, 109, 1–15, https://doi.org/10.1029/2003jc002008, 2004.
 - Fretwell, P., Pritchard, H. D., Vaughan, D. G., Bamber, J. L., Barrand, N. E., Bell, R., Bianchi, C., Bingham, R. G., Blankenship, D. D., Casassa, G., Catania, G., Callens, D., Conway, H., Cook, A. J., Corr, H. F., Damaske, D., Damm, V., Ferraccioli, F., Forsberg, R., Fujita, S., Gim, Y., Gogineni, P., Griggs, J. A., Hindmarsh, R. C., Holmlund, P., Holt, J. W., Jacobel, R. W., Jenkins, A., Jokat, W., Jordan, T., King,
- E. C., Kohler, J., Krabill, W., Riger-Kusk, M., Langley, K. A., Leitchenkov, G., Leuschen, C., Luyendyk, B. P., Matsuoka, K., Mouginot, J., Nitsche, F. O., Nogi, Y., Nost, O. A., Popov, S. V., Rignot, E., Rippin, D. M., Rivera, A., Roberts, J., Ross, N., Siegert, M. J., Smith, A. M., Steinhage, D., Studinger, M., Sun, B., Tinto, B. K., Welch, B. C., Wilson, D., Young, D. A., Xiangbin, C., and Zirizzotti, A.: Bedmap2: Improved ice bed, surface and thickness datasets for Antarctica, Cryosphere, 7, 375–393, https://doi.org/10.5194/tc-7-375-2013, 2013.
 - Fretwell, P., Pritchard, H., Vaughan, D., Bamber, J., Barrand, N., Bell, R. E., Bianchi, C., Bingham, R., Blankenship, D., Casassa, G., Catania,
- G., Callens, D., Conway, H., Cook, A., Corr, H., Damaske, D., Damn, V., Ferraccioli, F., Forsberg, R., and ... Bodart, J.: BEDMAP2 Ice thickness, bed and surface elevation for Antarctica standardised shapefiles and geopackages (Version 1.0) [Data set], NERC EDS UK Polar Data Centre, https://doi.org/https://doi.org/10.5285/0f90d926-99ce-43c9-b536-0c7791d1728b, 2022.
 - Gade, H. G.: Melting of Ice Sea Water: A Primitive Model with Application to the Antarctic Ice Shelf and Icebergs, Journal of Physical Oceanography, pp. 189–198, https://doi.org/10.1175/1520-0485(1979)009<0189:MOIISW>2.0.CO;2, 1979.
- 600 Gill, A. E.: Circulation and bottom water production in the Weddell Sea, Deep-Sea Research and Oceanographic Abstracts, 20, 111–140, https://doi.org/10.1016/0011-7471(73)90048-X, 1973.
 - Hattermann, T.: Antarctic thermocline dynamics along a narrow shelf with easterly winds, Journal of Physical Oceanography, 48, 2419–2443, https://doi.org/10.1175/JPO-D-18-0064.1, 2018.
- Hattermann, T., Nicholls, K. W., Hellmer, H. H., Davis, P. E. D., Janout, M., Østerhus, S., Schlosser, E., Rohardt, G., and Kanzow, T.:

 Observed interannual changes beneath Filchner- Ronne Ice Shelf linked to large-scale atmospheric circulation, Nature Communications,
 12, 1–11, https://doi.org/10.1038/s41467-021-23131-x, 2021.
 - Hazel, J. E. and Stewart, A. L.: Are the near-Antarctic easterly winds weakening in response to enhancement of the southern annular mode?, Journal of Climate, 32, 1895–1918, https://doi.org/10.1175/JCLI-D-18-0402.1, 2019.
- Hellmer, H. H., Kauker, F., Timmermann, R., Determann, J., and Rae, J.: Twenty-first-century warming of a large Antarctic ice-shelf cavity by a redirected coastal current, Nature, 485, 225–228, https://doi.org/10.1038/nature11064, 2012.
 - Hellmer, H. H., Kauker, F., Timmermann, R., and Hattermann, T.: The fate of the Southern Weddell sea continental shelf in a warming climate, Journal of Climate, 30, 4337–4350, https://doi.org/10.1175/JCLI-D-16-0420.1, 2017.
 - Hersbach, H., Bell, B., Berrisford, P., Horányi, A., Sabater, J. M., Nicolas, J., Radu, R., Schepers, D., Simmons, A., Soci, C., and Dee, D.: Global reanalysis: goodbye ERA-Interim, hello ERA5, ECMWF Newsletter, pp. 17–24, 2019.
- Hersbach, H., Bell, B., Berrisford, P., Biavati, G., Horányi, A., Muñoz Sabater, J., Nicolas, J., Peubey, C., Radu, R., Rozum, I., Schepers, D., Simmons, A., Soci, C., Dee, D., and Thépaut, J.-N.: ERA5 hourly data on single levels from 1940 to present. [Data set] (Accessed on 08-

- 02-2023), Copernicus Climate Change Service (C3S) Climate Data Store (CDS), https://doi.org/https://doi.org/10.24381/cds.adbb2d47, 2023.
- Jacobs, S. S.: On the nature and significance of the Antarctic Slope Front, Marine Chemistry, 35, 9–24, https://doi.org/10.1016/S0304-620 4203(09)90005-6, 1991.
 - Jacobs, S. S.: Bottom water production and its links with the thermohaline circulation, Antarctic Science, 16, 427–437, https://doi.org/10.1017/S095410200400224X, 2004.
 - Janout, M., Hellmer, H. H., Hattermann, T., Huhn, O., Sültenfuss, J., Østerhus, S., Stulic, L., Ryan, S., Schröder, M., and Kanzow, T.: FRIS Revisited in 2018: On the Circulation and Water Masses at the Filchner and Ronne Ice Shelves in the Southern Weddell Sea, Journal of Geophysical Research: Oceans, 126, 1–19, https://doi.org/10.1029/2021JC017269, 2021.
 - Janout, M. A., Hellmer, H. H., and Monsees, M.: Raw data of physical oceanography and current velocity data from moorings AWI252-3, AWI253-3 and AWI254-3 in Filchner Trough, February 2018 March 2021, https://doi.org/10.1594/PANGAEA.944430, 2022.
 - Jensen, M. F., Fer, I., and Darelius, E.: Low frequency variability on the continental slope of the southern Weddell Sea, Journal of Geophysical Research: Oceans, 118, 4256–4272, https://doi.org/10.1002/jgrc.20309, 2013.
- 630 Lauber, J., Hattermann, T., de Steur, L., Darelius, E., Auger, M., Nøst, O. A., and Moholdt, G.: Warming beneath an East Antarctic ice shelf due to increased subpolar westerlies and reduced sea ice, Nature Geoscience, https://doi.org/10.1038/s41561-023-01273-5, 2023.
 - Marshall, J. and Speer, K.: Closure of the meridional overturning circulation through Southern Ocean upwelling, Nature Geoscience, 5, 171–180, https://doi.org/10.1038/ngeo1391, 2012.
- Martin, T., Steele, M., and Zhang, J.: Seasonality and long-term trend of Arctic Ocean surface stress in a model, Journal of Geophysical Research: Oceans, pp. 1723–1738, https://doi.org/10.1002/2013JC009425.Received, 2014.
 - Martin, T., Tsamados, M., Schroeder, D., and Feltham, D.: The impact of variable sea ice roughness on changes in Arctic Ocean surface stress: a model study, Journal of Geophysical Research: Oceans, 121, 1931–1952, https://doi.org/http://dx.doi.org/10.1002/2015JC011186, 2016.
 - McDougall, T. and Barker, P.: Getting started with TEOS-10 and the Gibbs Seawater (GSW) Oceanographic Toolbox, ISBN 9780646556215, 2011.
- Morrison, A. K., McC. Hogg, A., England, M. H., and Spence, P.: Warm Circumpolar Deep Water transport toward Antarctica driven by local dense water export in canyons, Science Advances, 6, 1–10, https://doi.org/10.1126/sciadv.aav2516, 2020.
 - Nicholls, K. W.: JR097 Cruise Report Autosub Under Ice Cruise to the southern Weddell Sea, https://www.bodc.ac.uk/resources/inventories/cruise inventory/reports/jr97 05.pdf, 2005.
 - Nicholls, K. W., Østerhus, S., Makinson, K., Gammelsrød, T., and Fahrbach, E.: Ice-ocean processes over the continental shelf of the southern Weddell Sea, Antarctica: A review, Reviews of Geophysics, 47, https://doi.org/10.1029/2007RG000250, 2009.
 - NSIDC: What are the EASE Grid., https://nsidc.org/data/ease, https://nsidc.org/data/ease, date Accessed: 2019-09-29, 2019.
 - NSIDC: How to convert the horizontal and vertical components to east and north, https://nsidc.org/data/user-resources/help-center/how-convert-horizontal-and-vertical-components-east-and-north, date accessed: 28 September 2024, 2024.
- Orsi, A. H., Johnson, G. C., and Bullister, J. L.: Circulation, mixing, and production of Antarctic Bottom Water, Progress in Oceanography, 43, 55–109, https://doi.org/10.1016/S0079-6611(99)00004-X, 1999.
 - Østerhus, S.: Physical oceanography and current velocity data from mooring S218E, 2024.

625

645

Ryan, S., Schröder, M., Huhn, O., and Timmermann, R.: On the warm inflow at the eastern boundary of the Weddell Gyre, Deep-Sea Research Part I: Oceanographic Research Papers, 107, 70–81, https://doi.org/10.1016/j.dsr.2015.11.002, 2016.

- Ryan, S., Hattermann, T., Darelius, E., and Schröder, M.: Seasonal cycle of hydrography on the eastern shelf of the Filchner Trough, Weddell Sea, Antarctica, Journal of Geophysical Research: Oceans, 122, 6437–6453, https://doi.org/10.1002/2017JC012916, 2017.
 - Sallée, J.-B., Vignes, L., Minière, A., Steiger, N., Pauthenet, E., Lourenco, A., Speer, K., Lazarevich, P., and Nicholls, K. W.: Subsurface floats in the Filchner Trough provide the first direct under-ice tracks of the circulation on shelf, Ocean Science, 20, 1267–1280, https://doi.org/10.5194/os-20-1267-2024, 2024.
- Semper, S. and Darelius, E.: Seasonal resonance of diurnal coastal trapped waves in the southern Weddel Sea, Antarctica, Ocean Science, 13, 77–93, https://doi.org/10.5194/os-13-77-2017, 2017.
 - Shchepetkin, A. F. and McWilliams, J. C.: Computational Kernel Algorithms for Fine-Scale, Multiprocess, Longtime Oceanic Simulations, Handbook of Numerical Analysis, 14, 121–183, https://doi.org/10.1016/S1570-8659(08)01202-0, 2009.
 - Steele, M., Zhang, J., Rothrock, D., and Stern, H.: The force balance of sea ice in a numerical model of the Arctic Ocean, Journal of Geophysical Research: Oceans, 102, 21 061–21 079, https://doi.org/10.1029/97JC01454, 1997.
- Steiger, N. and J.-B., S.: Hydrological and current velocity data from moorings P1, P2, P4, P5 and P6 in the Filchner Trough region in the southern Weddell Sea, February 2017 to March 2021., https://doi.org/https://doi.org/10.17882/100680, 2023.
 - Steiger, N., Sallée, J. B., Darelius, E., Janout, M., and Østerhus, S.: Observed Pathways and Interannual Variability of the Warm Inflow Onto the Continental Shelf in the Southern Weddell Sea, Journal of Geophysical Research: Oceans, 129, e2023JC020700, https://doi.org/https://doi.org/10.1029/2023JC020700, e2023JC020700 2023JC020700, 2024.
- Thompson, A. F., Stewart, A. L., Spence, P., and Heywood, K. J.: The Antarctic Slope Current in a Changing Climate, Reviews of Geophysics, 56, 741–770, https://doi.org/10.1029/2018RG000624, 2018.
 - Tsamados, M., Feltham, D. L., Schroeder, D., Flocco, D., Farrell, S. L., Kurtz, N., Laxon, S. W., and Bacon, S.: Impact of Variable Atmospheric and Oceanic Form Drag on Simulations of Arctic Sea Ice, Journal of Physical Oceanography, 44, 1329 1353, https://doi.org/10.1175/JPO-D-13-0215.1, 2014.
- Tschudi, M., Meier, W. N., Stewart, J. S., Fowler, C., and Maslanik, J.: Polar Pathfinder Daily 25 km EASE-Grid Sea Ice Motion Vectors, Version 4, https://doi.org/10.5067/INAWUWO7QH7B, 2019a.
 - Tschudi, M. A., Meier, W. N., and Stewart, J. S.: An enhancement to sea ice motion and age products, The Cryosphere Discussions, pp. 1–29, https://doi.org/10.5194/tc-2019-40, 2019b.
 - Wåhlin, A. K., Yuan, X., Bjork, G., and Nohr, C.: Inflow of Warm Circumpolar Deep Water in the Central Amundsen Shelf, Journal of Physical Oceanography, 40, 1427–1434, https://doi.org/10.1175/2010JPO4431.1, 2010.

680

Webb, D. J., Holmes, R. M., Spence, P., and England, M. H.: Barotropic Kelvin Wave-Induced Bottom Boundary Layer Warming Along the West Antarctic Peninsula, Journal of Geophysical Research: Oceans, 124, https://doi.org/https://doi.org/10.1029/2018JC014227, 2019.